



Characterization of Experimental Fracture Alteration and Fluid Flow in Fractured Natural Seals

25 August 2014

Disclaimer

This report was prepared as an account of work sponsored by an agency of the United States Government. Neither the United States Government nor any agency thereof, nor any of their employees, makes any warranty, express or implied, or assumes any legal liability or responsibility for the accuracy, completeness, or usefulness of any information, apparatus, product, or process disclosed, or represents that its use would not infringe privately owned rights. Reference therein to any specific commercial product, process, or service by trade name, trademark, manufacturer, or otherwise does not necessarily constitute or imply its endorsement, recommendation, or favoring by the United States Government or any agency thereof. The views and opinions of authors expressed therein do not necessarily state or reflect those of the United States Government or any agency thereof.

This report has been reviewed by NETL and approved for public release.

Cover Illustration: Medical computed tomography scanner at the National Energy Technology Laboratory (NETL) in Morgantown, WV with ancillary core flow apparatus, multiple ISCO pumps, and core holder shown in foreground. Photograph by Karl Jarvis.

Suggested Citation: Crandall, D.; Bromhal, G. *Characterization of Experimental Fracture Alteration and Fluid Flow in Fractured Natural Seals*; NRAP-TRS-III-003-2014; NRAP Technical Report Series; U.S. Department of Energy, National Energy Technology Laboratory: Morgantown, WV, 2014; p 48.

An electronic version of this report can be found at:
<http://www.netl.doe.gov/research/on-site-research/publications> and
<https://edx.netl.doe.gov/nrap>

Characterization of Experimental Fracture Alteration and Fluid Flow in Fractured Natural Seals

Dustin Crandall, Grant Bromhal

**U.S. Department of Energy, National Energy Technology Laboratory, 3610 Collins Ferry
Road, Morgantown, WV 256507**

NRAP-TRS-III-003-2014

Level III Technical Report Series

25 August 2014

This page intentionally left blank.

Table of Contents

EXECUTIVE SUMMARY	1
1. INTRODUCTION.....	2
2. SEAL FORMATIONS	6
2.1 KIRTLAND SHALE – SAN JUAN BASIN	6
2.2 EAU CLAIRE MUDSTONE – ILLINOIS BASIN.....	8
2.3 TUSCALOOSA CLAYSTONE – GULF COAST.....	10
3. METHODS.....	12
3.1 COMPUTED TOMOGRAPHY SCANNING.....	12
3.2 ADDITIONAL ANALYSIS.....	14
3.3 CT IMAGE ANALYSIS.....	16
4. RESULTS AND OBSERVATIONS.....	18
4.1 KIRTLAND SHALE	18
4.2 EAU CLAIRE MUDSTONE.....	23
5. DISCUSSION.....	35
5.1 KIRTLAND SHALE	35
5.2 EAU CLAIRE MUDSTONE.....	35
5.3 TUSCALOOSA CLAYSTONE	35
6. CONCLUSIONS	36
7. REFERENCES.....	37

List of Figures

Figure 1: Typical fracture geometry.	3
Figure 2: Preserved Upper Kirtland shale sample, as received at NETL.	6
Figure 3: Sub-cored Upper Kirtland shale sample.	7
Figure 4: Prepared sub-core of Upper Kirtland shale sample.	8
Figure 5: Eau Claire mudstone core, as received at NETL.	8
Figure 6: Eau Claire mudstone core samples with sub-cores.	9
Figure 7: Eau Claire fractured sub-core “B” sample.	10
Figure 8: Eau Claire fractured sub-core “D” sample.	10
Figure 9: Fractured Tuscaloosa core sample.	11
Figure 10: Medical CT scanner at NETL in Morgantown, WV with ancillary flow apparatus.	12
Figure 11: Medical CT scanner with Hassler-style core holder and ancillary flow apparatus.	13
Figure 12: Schematic of flow-through system with pumps and core holder.	14
Figure 13: The North Star Imaging M-5000 industrial CT scanner at NETL in Morgantown, WV.	15
Figure 14: The multi-sensor core logger at NETL in Morgantown, WV.	15
Figure 15: Greyscale CT slices of fractured Tuscaloosa claystone sample.	17
Figure 16: False color medical CT slices of fractured Kirtland shale sample, XY planes.	19
Figure 17: False color medical CT slices of fractured Kirtland shale sample, XZ planes.	19
Figure 18: Greyscale industrial CT scan reconstruction of fractured Kirtland shale sample.	20
Figure 19: Volume of effluent in the receiving pump for the fractured Kirtland shale test.	21
Figure 20: Calculated bulk density of the fractured Kirtland shale core.	21
Figure 21: Average bulk density of the Kirtland shale sample over the experiment.	22
Figure 22: Pre- and post-elemental constituents in the brine used for the Kirtland shale fractured flow test.	22
Figure 23: False color medical CT slice of full Eau Claire mudstone core, XZ plane.	23
Figure 24: Greyscale industrial CT slice of full Eau Claire mudstone core, XZ plane.	24
Figure 25: XRF measurements of the full Eau Claire mudstone core.	24
Figure 26: Slices of the medical CT scanner reconstruction of Eau Claire mudstone sub-core #1, XY plane.	25

Figure 27: 3-D reconstruction of an industrial CT scan of the fracture in the Eau Claire mudstone sub-core #1.	26
Figure 28: Averaged bulk dual-energy derived density of the entire of the Eau Claire sub-core #1.....	27
Figure 29: Fracture region of interest (shown in yellow) for analysis of Eau Claire sub-core #1.....	27
Figure 30: Averaged bulk dual-energy derived density of the smaller region of interest of the Eau Claire sub-core #1.....	28
Figure 31: Slices of the medical CT scanner reconstruction of Eau Claire mudstone sub-core #2, XY plane.	29
Figure 32: Slices of the medical CT scanner reconstruction of Eau Claire mudstone sub-core #2, XZ plane.....	29
Figure 33: Averaged bulk dual-energy derived density of the entire Eau Claire sub-core #2.....	30
Figure 34: Pressure across Eau Claire sub-core #2, measured from 0–250 psi differential pressure gauge.....	31
Figure 35: False color medical CT slices of fractured Tuscaloosa claystone sample, XY planes.	32
Figure 36: False color medical CT slices of fractured Tuscaloosa claystone sample, XZ planes.	32
Figure 37: Averaged bulk dual-energy derived density of the Tuscaloosa claystone.	33
Figure 38: Pressure across the Tuscaloosa fractured core, measured from 0–250 psi differential pressure gauge.....	34

List of Tables

Table 1: Kirtland shale brine recipe.....	7
Table 2: Eau Claire mudstone brine recipe.....	9
Table 3: Tuscaloosa claystone brine recipe	11
Table 4: Experimental parameters of flow-through tests.....	18

Acronyms, Abbreviations, and Symbols

Term	Description
ϕ	Porosity
k	Permeability
2-D	Two-dimensional
3-D	Three-dimensional
CCUS	Carbon capture utilization and storage
CO ₂	Carbon dioxide
CT	Computed tomography
CTN	Computed tomography number
DOE	Department of Energy
LANL	Los Alamos National Laboratory
LBNL	Lawrence Berkeley National Laboratory
LLNL	Lawrence Livermore National Laboratory
MSCL	Multi-sensor core logger
NETL	National Energy Technology Laboratory
NRAP	National Risk Assessment Partnership
PNNL	Pacific Northwest National Laboratory
ROM	Reduced-order model
SECARB	Southeast Regional Carbon Sequestration Partnership
USGS	United States Geological Survey
XRF	X-ray fluorescence

Acknowledgments

This work was completed as part of the National Risk Assessment Partnership (NRAP) project. Support for this project came from the Department of Energy's (DOE) Office of Fossil Energy's Crosscutting Research program. This work was funded as part of the American Recovery and Reinvestment Act of 2009. The authors wish to acknowledge Robert Romanosky (NETL Strategic Center for Coal) and Regis Conrad (DOE Office of Fossil Energy) for programmatic guidance, direction, and support.

The authors also wish to acknowledge Bryan Tennant, Karl Jarvis, and Roger Lapeer for operating the CT scanner lab. Thank you to Jinesh Jain and Neal Julien for ICP analysis; to Magdalena Gill for assistance with CT scanning analysis discussions; Hang Deng and Catherine A. Peters for assistance with the Eau Claire flow test results and setup; Dustin McIntyre for assistance with NETL's computed tomography lab; Pacific Northwest National Laboratory (PNNL) and Jeff Hoffman (NETL) for the Eau Claire samples; Jason Heath for the Kirtland shale sample; and Craig Griffith for the Tuscaloosa sample.

This page intentionally left blank.

EXECUTIVE SUMMARY

This report describes a series of experiments designed to examine the effects and flow of carbon dioxide (CO₂) saturated brine moving through samples from rock formations that are seals for geologic storage of CO₂. The samples were obtained from three sites being considered or used for carbon capture utilization and storage (CCUS) pilot studies within the continental United States. All samples contain small fractures (some natural, others induced) that make the samples suitable for examining the effects on seal integrity of seepage through small fractures.

Experiments were performed over multiple weeks by injecting CO₂-saturated brine through fractured samples while the samples were scanned with a computed tomography (CT) scanner at regular intervals during the course of the experiment. Representative reservoir pressures were maintained on the samples during the experiments. The goal was to evaluate the change in the fracture flow that would result from a CO₂ leak so that accurate relationships can be described in reduced-order models (ROMs) currently under development in the National Risk Assessment Partnership (NRAP) project.

Of the three formations studied, only one formation had a reaction that was significant. Reactions within the Tuscaloosa claystone sample appeared to reduce the transmissivity of the fracture slightly during the 39-day experiment. A change in the geometry of the fracture was not observable with the medical CT images that were captured during the experiment. All other tests showed minimal changes in the fractures and fracture flow properties.

These results indicate that geochemical reactions may not be significant within fractured seal formations *that contain the types of shale rock matrices used here*, and accounting for these reactions should not be needed in the ROMs being developed for the NRAP project. If a rock matrix contains minerals that are more reactive than the three samples studied here, this conclusion may not apply.

1. INTRODUCTION

Since the industrial revolution the amount of carbon dioxide (CO₂) in the atmosphere has risen at an unprecedented rate, resulting in global warming and climate change (ICCP, 2007). As a potential means to reduce the anthropogenic CO₂ released to the atmosphere, geologic CO₂ sequestration is being actively examined. Geologic CO₂ sequestration involves pumping CO₂ far below the surface of the earth into high permeability (k) and high porosity (ϕ) reservoirs. To keep the injected CO₂ within these reservoirs, there must be at least one low k and low ϕ formation above the reservoir to serve as a seal and thereby inhibit the vertical migration of the CO₂ toward the surface. Numerical simulations, cost benefit analyses, and field tests are all underway to determine the feasibility of carbon capture utilization and storage (CCUS) as a greenhouse gas mitigation activity. For CCUS to have a meaningful effect on climate change and the percent of CO₂ in the atmosphere, the CO₂ must remain in the subsurface for 100's to 1000's of years (ICCP, 2007). One concern about the long term viability of storage locations is the presence of fractures in the low k seal rock above the CO₂ reservoirs and the potential for these fractures to allow CO₂ leakage toward the surface.

An effort is underway to develop a tool that will provide accessible, science-based, and rapid assessment of potential geologic sequestration locations and scenarios. This effort, known as the National Risk Assessment Partnership (NRAP), combines expertise from Lawrence Berkley National Laboratory (LBNL), Lawrence Livermore National Laboratory (LLNL), Los Alamos National Laboratory (LANL), Pacific Northwest National Laboratory (PNNL), and the National Energy Technology Laboratory (NETL). The complex and multi-faceted problem of evaluating the risk of a significant leak from a geologic storage or sequestration facility has been separated into five distinct activities: reservoir performance, migration pathways from the reservoir, groundwater contamination, induced seismicity, and system integration (Pawar et al., 2013). The first four of these activities are each being solved using a simplified numerical model that captures the relevant physical relationships with a reduced number of input parameters. These reduced-order models (ROMs) are fast and provide the backbone of the NRAP project, working together to form a numerical tool for the CCUS risk assessment community (Zhang and Pau, 2012). The work presented in this report is an experimental examination of some of the parameters and relationships being used in a ROM for the seal, where a compromised sealing rock could enable significant vertical flow of CO₂ from a storage reservoir.

Flow through rock fractures has been a research topic of interest for decades (Zimmerman and Bodvarsson, 1996; Berkowitz, 2002). Analytical models were developed for laminar, single-phase fluid flow in a narrow fracture, bounded by impermeable walls, by simplifying the Navier-Stokes equations of fluid continuity:

$$\rho g_i - \frac{\partial P}{\partial x_i} + \mu \left(\frac{\partial^2 u_i}{\partial x_i^2} + \frac{\partial^2 u_i}{\partial x_j^2} + \frac{\partial^2 u_i}{\partial x_k^2} \right) = \rho \frac{\partial u_i}{\partial t} \quad (1)$$

where ρ is the fluid density, g_i = gravity in the x_i direction, P is the pressure, u_i is the fluid velocity in the x_i direction, t is time, and subscripts i, j and k are the three orthogonal primary directions. A typical vertical fracture geometry is shown in Figure 1 where the aperture, b , is much less than the fracture width, W , and length, L .

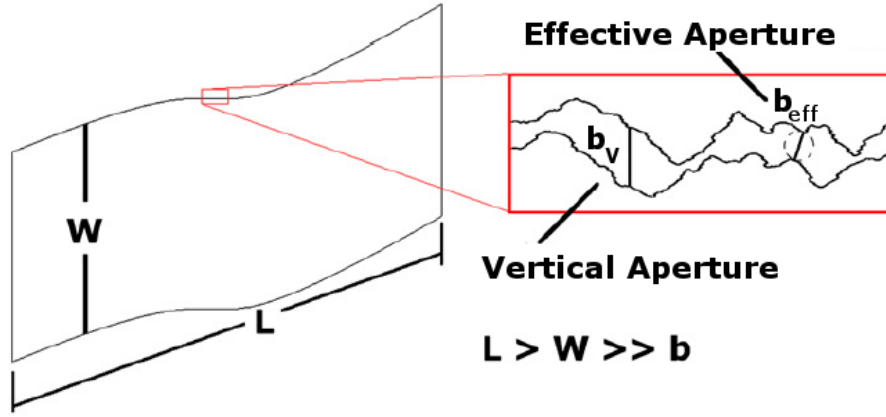


Figure 1: Typical fracture geometry.

By assuming that flow is steady, that temperature changes along the flow path are negligible (constant fluid properties), flow is perpendicular to gravitational forces, and that the fracture length, L , is large, Equation 1 reduces to:

$$\mu \left(\frac{\partial^2 u_i}{\partial x_j^2} \right) = \frac{\partial P}{\partial x_i} \quad (2)$$

Recognizing that the change in velocity (u_i) perpendicular to the flow direction (x_j) at $\frac{1}{2}b$ is zero and that no slip boundaries exist at the fracture walls, a solution to Equation 2 can be found and integrated over the fracture b such that:

$$Q = -\frac{Wb^3}{12\mu} \frac{\Delta P}{L} \quad (3)$$

where Q is the integrated mass flow through the fracture, and μ is the dynamic viscosity of the fluid. Equation 3 is commonly referred to as the “cubic law” of flow in fractures.

Experimentally the cubic law has been shown to be accurate when $b \ll W$, $b \ll L$, fracture wall roughness is small, the flow is laminar, the fluid acts in a Newtonian fashion, and $Re < 2400$, where Re is defined as (Witherspoon et al., 1980):

$$Re = \frac{Dv\rho}{\mu} \quad (4)$$

where D is the hydraulic diameter and is equal to four times the hydraulic radius.

There is a similarity of the cubic law to Darcy’s law for flow through porous media (Bear, 1972):

$$Q = k \frac{A \Delta P}{\mu L} \quad (5)$$

where k is the permeability of the porous medium and A is the cross-sectional area of the porous medium perpendicular to flow. Assuming that the A of a fracture is equal to $W*b$, a definition of a fracture permeability, $k_{fracture}$, for smooth-walled fractures is (Witherspoon et al., 1979):

$$k_{fracture} = \frac{b^2}{12} \quad (6)$$

Often it is more convenient to measure a combined transmissivity (T), where T :

$$T = k_{fracture}A \quad (7)$$

where A is the mean of the fracture area perpendicular to the flow direction. Because the b of a fracture varies, the measurement of a combined T avoids having to calculate an average b for the A calculation, and permits an equivalent hydraulic aperture, b_H , to be calculated for use in discrete fracture flow models:

$$b_H^3 = \frac{12T}{W} \quad (8)$$

As is shown in Figure 1, the mechanical b can be defined in several ways, for example, as the distance between fracture surfaces perpendicular to the overall direction of flow, b_v , or as the largest distance that can be inscribed within the fracture walls at a given location, an effective (or perpendicular) aperture, b_{eff} . In the remainder of this report b is used to designate a physical measurement of the spacing between fracture walls and b_H is used to designate the flow relationship shown in Equation 8. Previous studies (Pyrak-Nolte et al., 1988; Konzuk & Kueper, 2004; Crandall et al., 2010) have shown that for a rough-walled fracture $b_H < b_v$ and $b_H < b_{eff}$, but the difference between the b_v and b_{eff} is not as great as the difference with the b_H .

Numerous studies have shown that applying an external force to a fractured core can reduce the b and b_H (Witherspoon et al., 1980; Pyrak-Nolte and Morris, 2000). This has been shown to be due primarily to the increase in zero-aperture locations, or contact zones, within the fractures (Walsh, 1981; Zimmerman et al., 1992). An increase in the contact locations increases the tortuosity of fluids moving through the fracture, which increases the length individual fluid particles must travel to traverse the macroscopic fracture length. Increasing the contact between fracture walls also creates more restrictive flow paths through the fracture. Both of these effects reduce the T of the fracture.

In a similar fashion, changes due to chemical interactions between the fluid in a fracture and the fracture surface can have an effect on the b and b_H . Numerical studies of reactive rocks and low pH fluid have shown significant increases in T (Li et al., 2008). Experimental studies have shown that low pH solutions can dissolve carbonates from rock fracture walls and increase T (Gouze et al., 2003; Detwiler and Rajaram, 2007; Noiriél et al., 2009). Conversely, experiments have shown that dissolution of fracture surfaces can decrease the b and b_H (Durham et al., 2001). The complex interactions between these geochemical reactions and the T of a fracture are of importance when considering CO₂ leakage from geologic reservoirs. Site specific fracture and fluid reactions can have different effects on the geometry and flow properties of fractures.

When CO₂ is injected into a geologic reservoir it will mix with the in-place or native fluid, often brine. The resultant plume of CO₂-saturated brine will have a lower pH than the non-saturated brine and has the potential to react with rocks within the seal, reservoir, and in the wellbore. Huerta et al. (2013) have shown a complex relationship with sealing occurring in long fractures of wellbore cement when a low-pH fluid migrates through the void. Deng et al. (2013a) and Ellis et al. (2011) have shown that when the rock fracture has a varied composition the more reactive

zones of minerals on the fracture walls will tend to dissolve in low pH environments and increase the b , but this has been shown to minimally affect the b_H , similar to what has been observed in reactive flow in natural porous media (Peters, 2009). Again, a complex interaction between the site specific fractured rock mass and the fluids migrating through the fracture can result in different interactions that will affect the T through fractures.

The current study is an examination of CO₂-saturated-brine flowing through a fracture in rock samples from a seal at three sites that are being considered or are actively being used for CCUS pilot studies within the continental United States. The experiments were performed over multiple weeks by injecting CO₂-saturated brine through fractured samples, which were scanned with a computed tomography (CT) scanner at regular intervals over the course of the experiment while kept at representative reservoir pressures. The goal was to evaluate the change in T that would result from a CO₂ leakage event so that accurate relationships can be implemented in ROMs being developed for seals under the NRAP project.

The remainder of the report is organized as follows. A discussion of the seals is given first, including brine composition, reservoir conditions, and location. Experimental details follow. The analysis methodology used to evaluate changes in the fractures during these experiments is given next, followed by a presentation of the results and a discussion of what these results mean for geologic storage of CO₂ and the development of a ROM for a seal layer.

2. SEAL FORMATIONS

Three cores from sealing formations from active or proposed CO₂ injections in the continental United States were acquired, fractured (if not naturally or previously fractured), and used for experiments on CO₂-saturated brine flow over periods of several weeks. A short description follows below on the formation rock and the locations of the CO₂ injection sites.

2.1 KIRTLAND SHALE – SAN JUAN BASIN

The Kirtland shale used for this study was acquired as a preserved core from injection well “EPNG Com A” at the Pump Canyon Site in the north central portion of the San Juan Basin, New Mexico (Heath et al., 2010). In October 2000, a multiple-year project with the Department of Energy (DOE) and industry partners was launched to evaluate the feasibility of CO₂ sequestration in unminable coal seams, including enhanced recovery of coal bed methane (Reeves, 2004). Since 2000, there have been several CO₂-sequestration pilot projects within the San Juan Basin, primarily focused on injection into the Fruitland Coal formation (Haerer and McPherson, 2009). Studies of fault locations, tracer movement, and the complex geology of the sealing formations above the Fruitland Coal (Wilson et al., 2012) indicate how these seals will react to CO₂-saturated-brine flow, which could be of importance when evaluating the long-term risk associated with storage here.

The sample used in this study was from a depth of 2,049 ft (624.5 m) which is in the Upper Kirtland shale formation (Heath et al., 2010). These samples were preserved by TerraTek after retrieving the core from the aluminum core sleeve with drilling mud, then wrapping layers of plastic, aluminum foil, and dipping in a core seal wax. The core was preserved within one month of drilling, and wrapped in plastic prior to the full sealing treatment so that the clays did not dry out (Keller, 2009). A photograph of this core, as received at NETL, is shown in Figure 2.



Figure 2: Preserved Upper Kirtland shale sample, as received at NETL.

The temperature and pressure conditions used for the Kirtland shale flow tests were calculated based on the DOE report by Heath et al. (2010) and heat flow records of the Fruitland coals (McCord et al., 1992). A pore pressure of 1,620 psi (11.17 MPa) and a core temperature of 27°C (80.6°F) were calculated from the reported pressure and temperature gradients, respectively. A simple brine was prepared according to a recipe (Table 1) based upon U.S. Geological Survey

(USGS) measurements of in situ brines at the depth from which this sample was obtained in the San Juan Basin.

Table 1: Kirtland shale brine recipe

Chemical	Molecular Weight	Grams per Liter Water
NaCl	58.443	17
KCl	74.552	0.295
MgCl ₂	95.212	0.075

Sub-coring of these samples was not simple due to the highly friable nature of the Kirtland shale. After attempts to sub-core the preserved sample using traditional core drills was shown to be non-effective, a 1.5-in. (3.81 cm) diameter sub-core was obtained with an OMAX Jet Machining Center, OMAX 2626 (OMAX Corp., Kent, WA). After the sample was sub-cored a thin layer of 5 Minute Epoxy (Devcon, Danvers, MA) was spread on the exposed surface, to protect against atmospheric degradation. This epoxy layer was allowed to fully cure and the sub-core was turned on a lathe to produce uniform and smooth sub-cores for the flow study. An image of the Kirtland shale sub-core directly after being removed from the preserved core is shown in Figure 3. The final prepared sub-core of the Upper Kirtland shale is shown in Figure 4. The friable nature of the Kirtland shale and the unique sub-coring process resulted in a competent fractured core.



Figure 3: Sub-cored Upper Kirtland shale sample.



Figure 4: Prepared sub-core of Upper Kirtland shale sample.

2.2 EAU CLAIRE MUDSTONE – ILLINOIS BASIN

The Eau Claire mudstone sample used for this study was acquired as part of the ongoing FutureGen 2.0 characterization from well FGA#1 in Morgan County Illinois (Sullivan et al., 2012). The Eau Claire overlies the Mount Simon sandstone, a large formation with an estimated CO₂ storage potential between 16,900 and 67,600 MMT of CO₂ (NETL, 2012). The Mount Simon sandstone has a high ϕ , high k , large areal extent, is thick, and is located in a region with many high-volume point sources of CO₂ (NETL, 2012; Sullivan et al., 2012; Carroll et al., 2012). With the large potential for CCUS activities involving the Mount Simon sandstone, understanding how CO₂-saturated-brine interacts with the Eau Claire formation could be critical for risk assessments.

The portion of the Eau Claire studied here was obtained from a depth of 3,854 ft (1174.7 m), and the sample was collected as part of a well characterization performed by PNNL (Sullivan et al., 2012) with the assistance of Core Laboratories (Houston, TX). This sample is from the bottom of the Lombard member, a primary seal for the Mount Simon sandstone. The sample as received at NETL is shown in Figure 5.

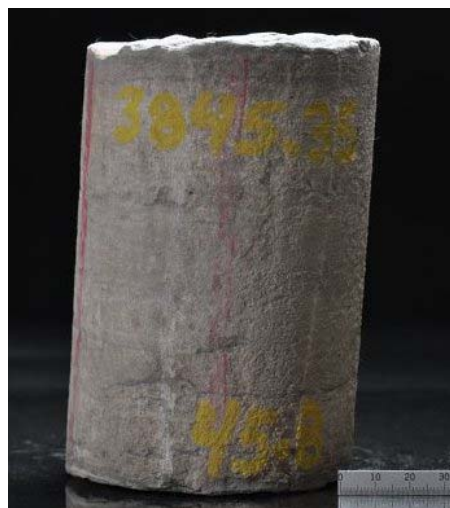


Figure 5: Eau Claire mudstone core, as received at NETL.

In-situ pressure was calculated to be approximately 1,850 psi based on published literature (Sullivan et al., 2012) and the depth of the retrieved core. A confining pressure of 1,850 psi was maintained during the Eau Claire fracture flow experiments with fluid pressures that varied between 1,600 and 1,700 psi (constant fluid injection rate). The brine recipe listed in Table 2 was determined by Deng et al. (2013b), based on the work of Liu et al. (2012).

Table 2: Eau Claire mudstone brine recipe

Chemical	Molecular Weight	Mole per kgw	Grams per Liter Water
NaCl	58.443	1.594E+00	93.174
KCl	74.552	3.108E-02	2.317
CaCl ₂	110.985	3.547E-01	39.366
MgCl ₂	95.212	8.922E-02	8.495
MgSO ₄	120.368	1.408E-02	1.695
NaHCO ₃	84.007	1.724E-03	0.145

The 6-in. long sample of the Eau Claire mudstone was sub-cored using standard core drills to make 1-in. (2.54 cm) diameter samples. The resultant cores were competent as shown in Figure 6. Because the sub-cores lacked visible natural fractures, each sub-core needed to have a fracture mechanically induced to provide a flow path. This fracture was induced perpendicular to the bedding planes using a modified Brazilian technique at NETL Pittsburgh (Fazio, 2012). Two samples were selected to perform the experimental flow tests, as shown in Figure 7 and Figure 8.



Figure 6: Eau Claire mudstone core samples with sub-cores.



Figure 7: Eau Claire fractured sub-core “B” sample.



Figure 8: Eau Claire fractured sub-core “D” sample.

2.3 TUSCALOOSA CLAYSTONE – GULF COAST

The Lower Tuscaloosa claystone used for this study was acquired from the Mississippi Test site of the Southeast Regional Carbon Sequestration Partnership (SECARB) (Griffith et al., 2011). The sample was cored at a depth of 8,569.75 ft (2,612 m) from well HH-38927 located at Mississippi Power’s Plant Daniel near Escatawpa, Mississippi in Jackson County. The purpose of this SECARB test was to identify and validate the CO₂ storage potential of deep saline reservoirs in the Gulf Coast region. Approximately 3,020 tons of CO₂ were successfully injected at the Plant Daniel site in 2008 (Brown, et al., 2013).

No photo is available to show this sample as received. A similar sample (3-50) from the same well is shown in Figure 9. The depth of the core and a standard pressure gradient was used to determine an appropriate confining pressure of 4,000 psi. The as-received sample was fractured. The sample appeared to have desiccated slightly and broke along several bedding planes. The 1.5-in. (3.81 cm) diameter and 2.5-in. (6.35 cm) long sample was coated with epoxy to ensure it

remained intact over the experiment, but no additional mechanical fracturing was needed. The experiment used a brine recipe (Table 3) based on supplemental data on brine composition presented by Lu et al. (2012).

Table 3: Tuscaloosa claystone brine recipe

Chemical	Molecular Weight	Mole per kgw	Grams per Liter Water
NaCl	58.443	1.88E+00	109.63
KCl	74.552	8.05E-03	0.60
CaCl ₂	110.985	2.92E-01	32.40
MgCl ₂	95.212	4.34E-02	4.13
NaBr	102.893	5.15E-03	0.53
Cl ₂ Sr	158.526	7.87E-03	1.25



Figure 9: Fractured Tuscaloosa core sample.

3. METHODS

All flow tests discussed in this report were performed in the medical CT scanner facility at NETL in Morgantown, WV. The fractured seal samples used were from the three sites previously discussed. Basic operation and properties of the CT scanners and scans are reviewed here, followed by more detailed test conditions, and additional analysis that were performed in conjunction with the standard CT scanning tests.

3.1 COMPUTED TOMOGRAPHY SCANNING

NETL's Universal Systems HD350-E 4th-generation refurbished medical CT scanner with 4,800 detectors and one rotating X-ray source was used to non-destructively image the internal structure of the fractured cores. This scanner is capable of operating at 140 kV and 400 mA, has a maximum resolution in the x-y plane (perpendicular to the core length) of 0.25 mm ($9.84(10^{-3})$ in.) and 1 mm ($3.94(10^{-2})$ in.) along the axial direction. NETL's medical scanner is shown in Figure 10 with ancillary flow equipment (i.e. pressure transducers, injection tubing, and tubing frame on the CT scanner bed). The same system is shown in Figure 11 with four Isco pumps (Teledyne Isco, Lincoln Nebraska) in foreground and a Hassler-style core holder (Core Laboratories, Tulsa Oklahoma) that was used to contain the fractured core, while applying both axial and radial pressure to the core during flow tests.



Figure 10: Medical CT scanner at NETL in Morgantown, WV with ancillary flow apparatus.



Figure 11: Medical CT scanner with Hassler-style core holder and ancillary flow apparatus.

Dual-energy scanning was used to improve the computed tomography number (CTN) to density conversions that were used in these experiments. Dual-energy scanning is the process of scanning at two energy levels to maximize the Compton scattering effects at high energy and maximize the photoelectric adsorption effect at low scanning energies (Wellington and Vinegar, 1987). This has been used for several other studies at NETL where small changes within a geologic sample were being examined (Jikich et al., 2010; Santarosa et al., 2013). To calibrate the relationship between the CTN and density, several different materials with known density were scanned with the same CT scanning parameters as the fractured samples. These calibration samples included acrylic, nylon, Teflon, and other materials that are of similar density to geologic samples.

A Hassler-style pressure vessel was used to contain the fractured core during the flow tests. As is shown in Figure 11, the cylindrical core holder is placed in the center of the CT scanner orifice and moved through the X-ray field. This scanning was performed twice daily during standard working days (Monday through Friday) and once on the weekend days (Saturday and Sunday). The design of the core holder enables a confining pressure to be applied to the fractured sub-core while fluids are injected into the sample. A simplified diagram in Figure 12 shows how this system works. An Isco pump was used to increase the pressure of nitrogen gas in the annulus between the rubber sleeve containing the fractured core and the outside of the core holder. The value of this confining pressure was determined from the depth and estimated pressure gradient for each sample. Another Isco pump was used to inject a mixture of CO₂ and brine (labeled H₂O in Figure 12). A pressurized mixing vessel was used to keep the brine saturated with CO₂ prior to being injected into the core holder. On the backside of the core holder another Isco pump was used in the receiving mode to capture the fluids after they moved through the core. By using Isco pumps on the front and back of the system, a specified flow rate and approximate pressure gradient could be set, with additional controls used to ensure that the pressure inside of the core and rubber sleeve did not increase above the confining pressure. Brine and CO₂ was collected from the system through the use of a micro-metering valve connected to the system. Approximately 1 ml of solution was collected periodically to enable elemental brine analysis to be conducted after the experiment.

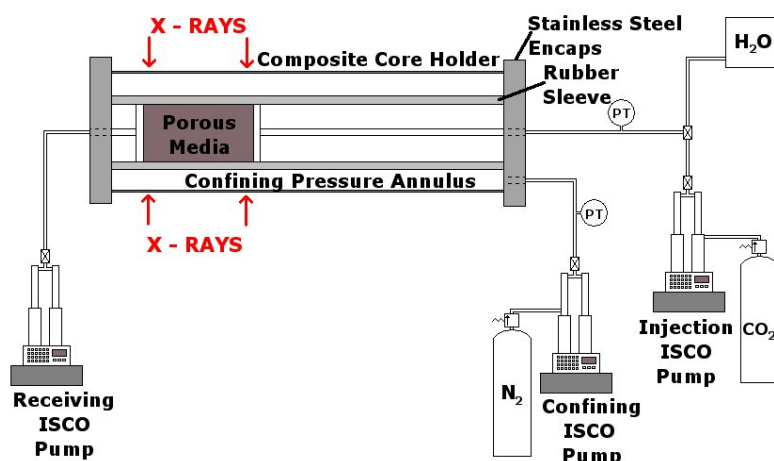


Figure 12: Schematic of flow-through system with pumps and core holder.

Injection flow rates and temperature of the system was varied for each experiment. For the first test, the flow, elevated temperature (80.6°F) and constant pressure at the injection side of the core (Kirtland shale) was tested. The temperature controllers were unwieldy and not used for the subsequent tests. The constant injection pressure resulted in unstable flow patterns, and collection of effluent from the exit side of the system was not possible at times. For the subsequent tests a constant injection rate was set with the Isco pumps and with additional software controls to ensure the pore pressure did not exceed the confining pressure. In this fashion, as long as the injection pressure was less than the confining pressure the flow rate was constant for a constant delta pressure. When the injection pressure increased to a value close to the confining pressure the flow rate was decreased to ensure safe operations.

A combination of LabView (National Instruments, Austin TX) instrument recordings, manual recording, and Isco pump recordings was used to capture the pressure and flow rate information during the experiments. Initially, LabView virtual instruments did a poor job of recording the data and frequently crashed with the first system that was installed in the laboratory. Flow results from the final tests are of higher quality due to the correction of various data collection issues.

3.2 ADDITIONAL ANALYSIS

The following additional analyses were performed when time and personnel were available.

3.2.1 Industrial CT Scanning

A North Star Imaging M-5000 industrial CT scanner at NETL in Morgantown, WV was used to view the fractured cores before and after the flow tests. Final testing followed a 1 year period of equipment setup, testing, and calibration. Therefore, there was a learning period throughout the year to determine the best parameters for scans. The final settings that resulted in the highest quality images were an X-ray source voltage of 180kV, X-ray current of 133.3 μ A, and an X-ray detector gain of 0.5 pF. For each three-dimensional (3-D) scan 1,440 projections were obtained as the sample rotated on the sample stage, with 5 radiographs averaged for each projection. With these conditions the reconstructed images of the 1-in. (2.54 cm) diameter cores in the Hassler core holder have a voxel resolution of 54.8 μ m. A photograph of the M-5000 industrial CT scanner is shown in Figure 13.

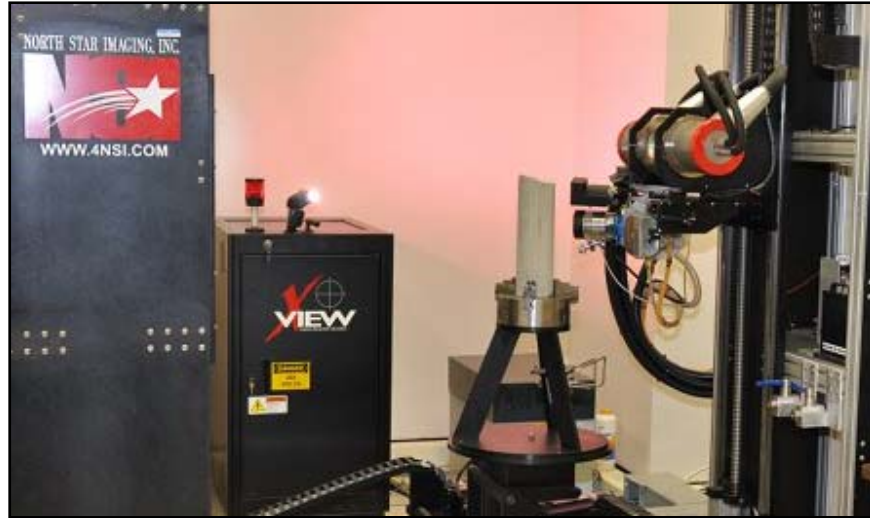


Figure 13: The North Star Imaging M-5000 industrial CT scanner at NETL in Morgantown, WV. X-ray source is shown on the right, a sandstone sample is vertically resting on the sample stage in the center, and the X-ray detector is on the left side of the photograph.

3.2.2 X-ray Fluorescence

A Geotek multi-sensor core logger (MSCL) at NETL has been used to measure various physical properties of geologic materials in a way that is comparable to borehole logging. The NETL logger is able to rapidly obtain high-resolution data including profiles of p-wave velocity, gamma-density, natural gamma ray emissions, resistivity, magnetic susceptibility, and X-ray fluorescence (XRF) from whole-round and split core samples. For our fracture flow studies, the only measurements of interest from the MSCL are the XRF, which were obtained with the handheld Innov-X (Olympus, Waltham, MA) X-Ray fluorescence spectrometer shown in Figure 14. XRF measurements of the sub-cores prior to coating with epoxy were taken for some samples to enable a more thorough understanding of the rock matrix properties.



Figure 14: The multi-sensor core logger at NETL in Morgantown, WV. Handheld XRF is the yellow device in the foreground.

3.3 CT IMAGE ANALYSIS

In X-ray CT, grayscale values of the final image are based on the amount of X-ray attenuation as the X-ray travels through matter. How much attenuation occurs in a given material is defined by the absorption coefficient, which is largely controlled by the density of the material. In practice absolute grayscale values can be further influenced by a range of environmental variables, and often vary from scan to scan. Experimental factors such as room temperature and how long the CT scanner has been running can influence the results. Additional factors are the atomic numbers of atoms in the attenuating material, and the energy of the penetrating X-rays, because absorption coefficients vary strongly with peak X-ray energy. Post-scan image processing requires scientific rigor to achieve consistent, repeatable, and statistically significant results.

To visualize fractures in the CT scanned images, low density (low CTN) zones of the core must be isolated via a grayscale threshold. Of the variety of automated thresholding processes that exist, many are based on histogram compilations of an entire image, which are then separated into two classes of pixels to create a binary image. For many geologic samples, image pixels can belong to more than two classes, representing more than two different materials (Arora et al., 2008; Osuna-Enciso et al., 2013). For the fractured seal rock scans these classes are, in order from highest to lowest CTN, dense particles in the rock matrix, the bulk of the rock matrix itself, and the fluids in the fracture void space. The relative amounts of each of these materials can skew a binary threshold histogram and cause an automated thresholding process to be affected. The variation in material that was observed in the CT scans can be seen in Figure 15, where two-dimensional (2-D) slices of a reconstructed medical CT scan of the fractured Tuscaloosa core are shown. In these grayscale CT images the darker regions indicate low density material, i.e. fractures. High-density matrix material can be observed in the slices as well; these are the brighter voxels within the images. The individual images shown in Figure 15 are one fourth of the image slices obtained from the medical CT images of the core; roughly 60 CT slices, 0.04-in. (1 mm) thick, comprise the digitally scanned core.

Additionally, occasional artifacts of the CT process can further skew the overall histogram. Artifacts can arise from high attenuation materials, reconstruction algorithm errors, and image acquisition oversights (Barrett and Keat, 2004). Often a careful examination of an image sequence by a human being is the most efficient way to detect image artifacts.

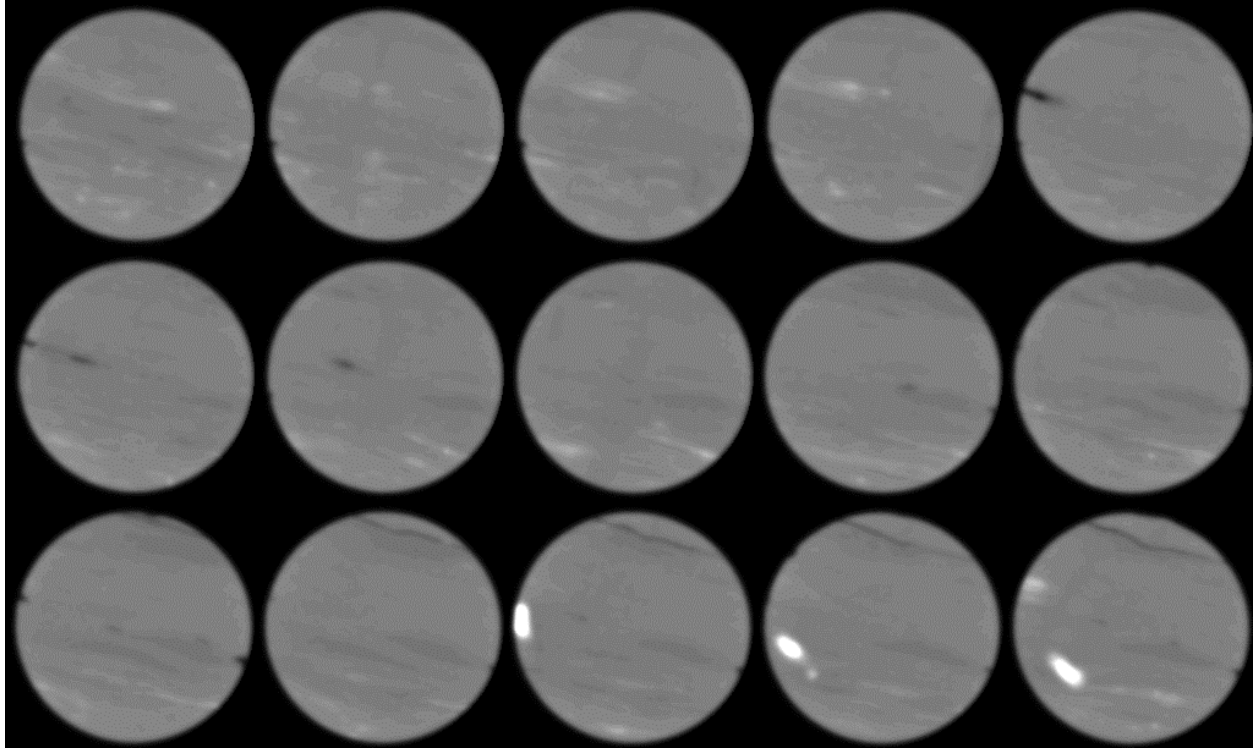


Figure 15: Greyscale CT slices of fractured Tuscaloosa claystone sample.

4. RESULTS AND OBSERVATIONS

Individual results from the four experiments performed on the three different fractured seal formations are described in this section. A review of the findings in common among the studied fractured seals is presented in the final sections of this report. Dates of the tests performed, pressure conditions, and injection rates are shown in Table 4. As can be seen in Table 4, flow was maintained for at least three weeks for all of these tests, with a maximum duration of 39 days for the fractured Tuscaloosa claystone sample.

Table 4: Experimental parameters of flow-through tests

Sample	Start Date	End Date	Number of Days	Confining Pressure (psi)	Maximum Pore Pressure (psi)	Injection Rate (ml/min)
Kirtland	1/12/2012	2/6/2012	25	1,850	1,620	$\approx 6.9(10^{-4})^*$
Eau Claire #1	9/4/2012	9/26/2012	22	1,850	1,650	0.013
Eau Claire #2	10/7/2012	10/26/2012	19	1,850	1,650	0.013/0.026
Tuscaloosa	12/21/2012	1/29/2013	39	4,000	3,750	0.013

*Constant pressure injection, flow rate varied.

4.1 KIRTLAND SHALE

Slices of a medical CT scan of the fractured Kirtland shale sample are shown in Figure 16 and Figure 17. These “slices”, and all other medical CT scanner slices in this document, were obtained from the raw 16-bit data files that were generated by the medical CT scanner’s reconstruction software. The reconstruction, which converted the X-ray attenuation data to the 3-D grayscale images, occurred inside the HD-350E software prior to researcher manipulation. Several features can be noted from Figure 16 and Figure 17.

- 1) The core is heterogeneous, with both high density zones (lighter regions) and fracture zones (darker regions) throughout the core
- 2) The fractures are small compared to the 0.25 mm x 0.25 mm x 1.0 mm voxel resolution of the medical CT images
- 3) The fracturing along the core is non-uniform. There is no discernible primary fluid pathway through the middle of the core as one would typically find in a standard mechanically fractured core. The geologic structure of the core and unique coring technique both contributed to this fracturing pattern.

With the above features noted, small changes in the structure of the fractures during the flow experiment would not be readily apparent.

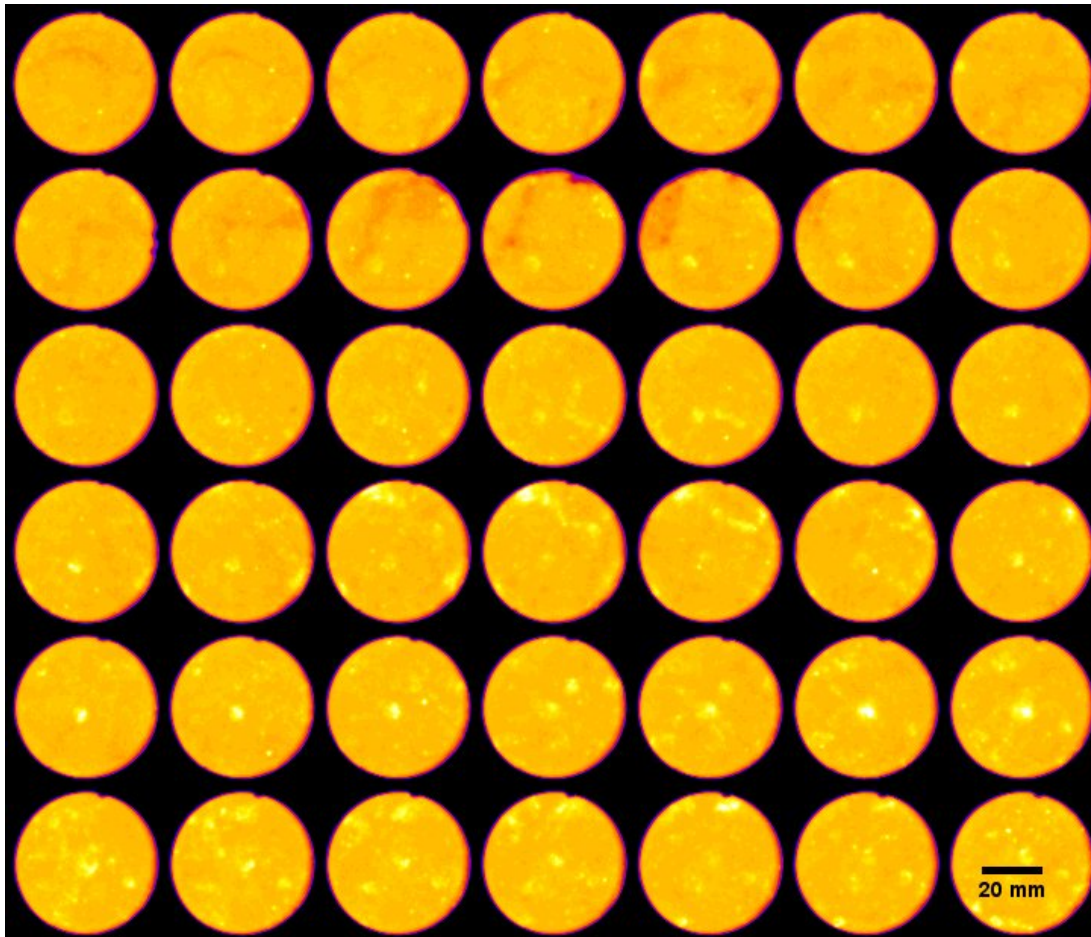


Figure 16: False color medical CT slices of fractured Kirtland shale sample, XY planes.

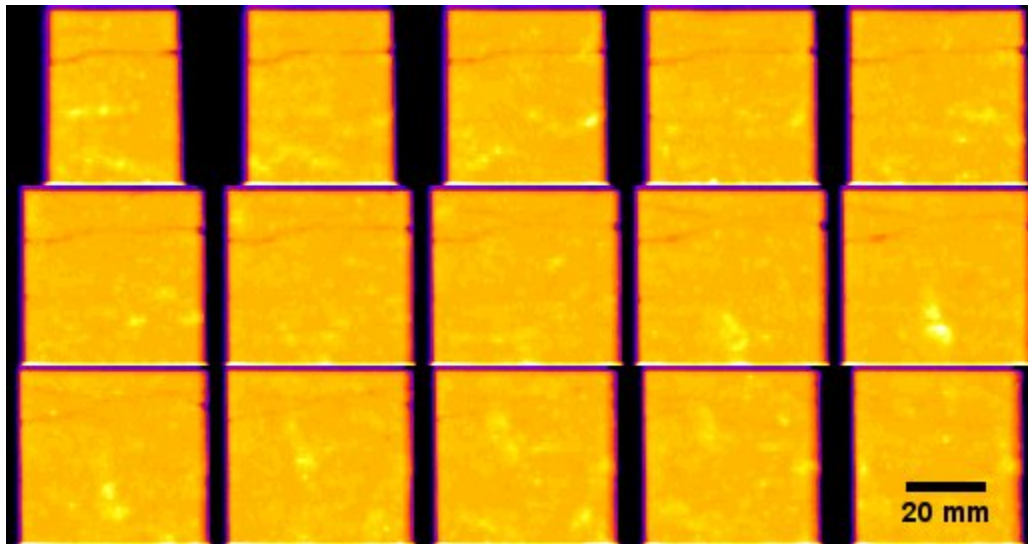


Figure 17: False color medical CT slices of fractured Kirtland shale sample, XZ planes.

An industrial CT scan of this core was performed as well. A slabbed 3-D reconstruction of this industrial CT scan is shown in Figure 18. The higher resolution of the industrial CT scan (57.9 micron, as opposed to 250 micron) reveals the connected fractures that span the core. The localized fracture zone along the edge of the core shown in Figure 18 is non-ideal for the bulk analysis that can be conducted in the medical CT scanner.

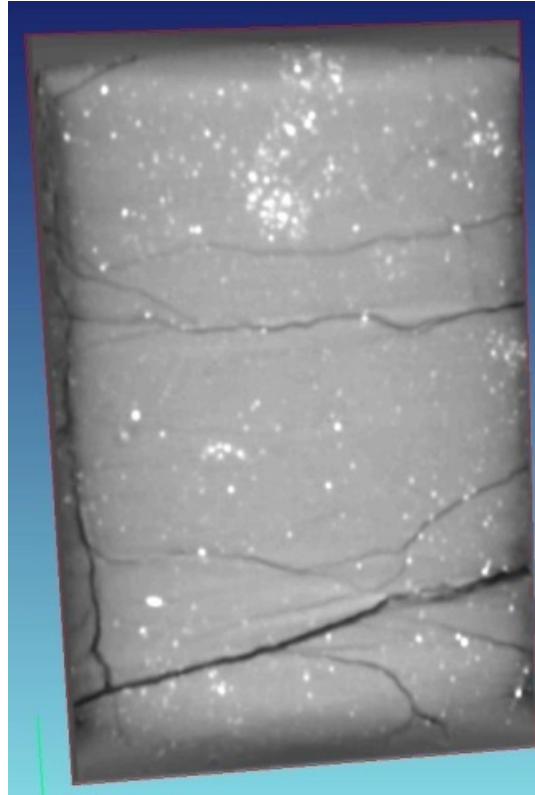


Figure 18: Greyscale industrial CT scan reconstruction of fractured Kirtland shale sample.

As mentioned previously, a constant pressure at the injection side of the core was held during this experiment. The LabView module intended to capture the pressure and flow information failed after several days. Written measurements of the volume of effluent in the downstream Isco pump were recorded over the remainder of the experiment. As is shown in Figure 19, bulk flow through the core remained fairly constant over the test duration. A flow rate of approximately 1 ml/day was maintained with a constant differential pressure across the core of -25 psi. No noticeable change in the relationship between differential pressure across the fractured core and the flow rate of brine was observed. This indicates that the permeability of the sample did not change appreciably over the course of the experiment. Examinations of the CT scans of this core over the course of the experiment appear to agree with this conclusion: there is no noticeable change in the fracture or core as determined by the CT images.

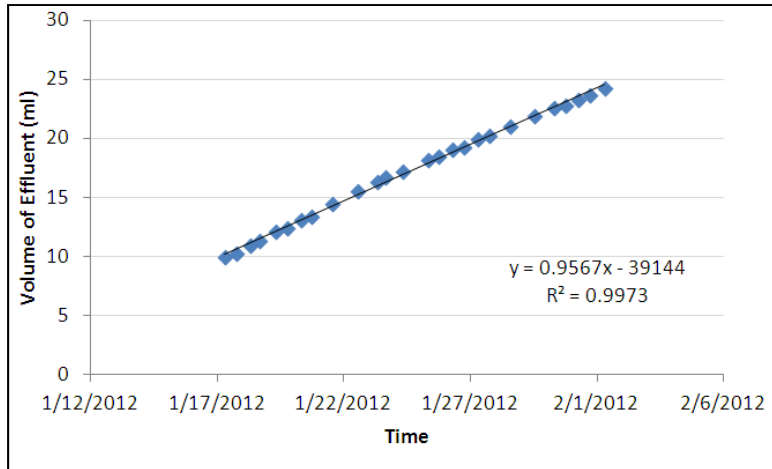


Figure 19: Volume of effluent in the receiving pump for the fractured Kirtland shale test.

The medical CT images were analyzed and converted to bulk density measurements by the use of dual-energy scanning conversion techniques (for details of this technique see Jikich et al. (2010)). The results of this bulk analysis reveal little systematic change in the density of the core during the 23-day experiment. As shown in Figure 20, the overall change in the bulk density of the core varied from 1.4 to 1.5 g/cm³ (or roughly 7%), but not in a systematic fashion that would indicate dissolution or precipitation within the sample. The average density of the Kirtland shale core as a function of date of scan is shown in Figure 21, and again no systematic change in the density can be noted that would conclusively indicate either precipitation or dissolution of the rock matrix around the fracture.

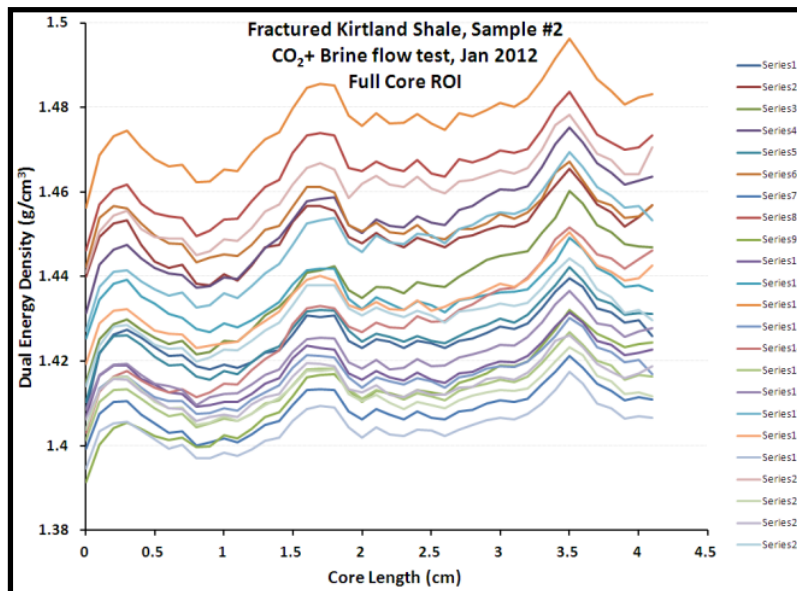


Figure 20: Calculated bulk density of the fractured Kirtland shale core.

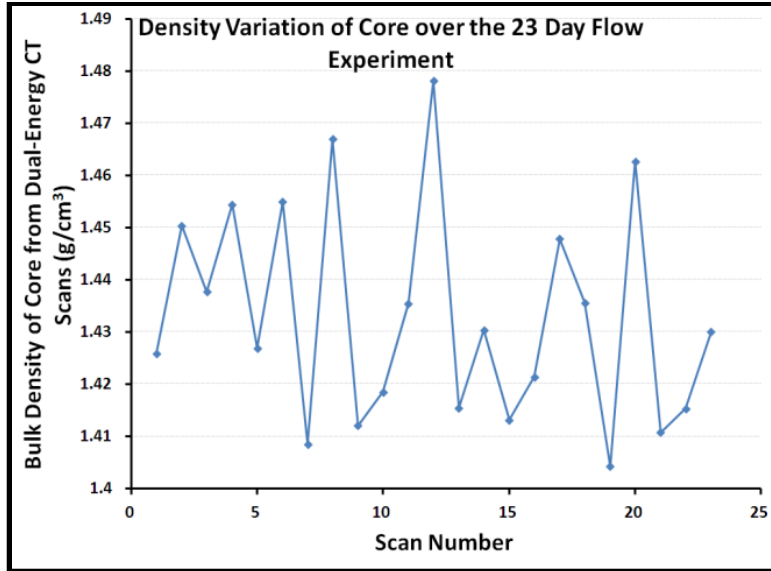


Figure 21: Average bulk density of the Kirtland shale sample over the experiment.

Brine samples that were saved for elemental analysis at the NETL Pittsburgh ICP-MS facility indicated that changes appear to have occurred, with an increase in Sr, Si, S, Na, Ca, Cu, and K and a decrease in the Mn, Ni, and Ti in the brine that has moved through the fractured core (Jain, 2012). Mg and Ca may also be precipitating out, as a small drop in these elements was observed. These results are shown in Figure 22. The total amount of change in the brine constituents was small, indicating a low amount of change within the fracture.

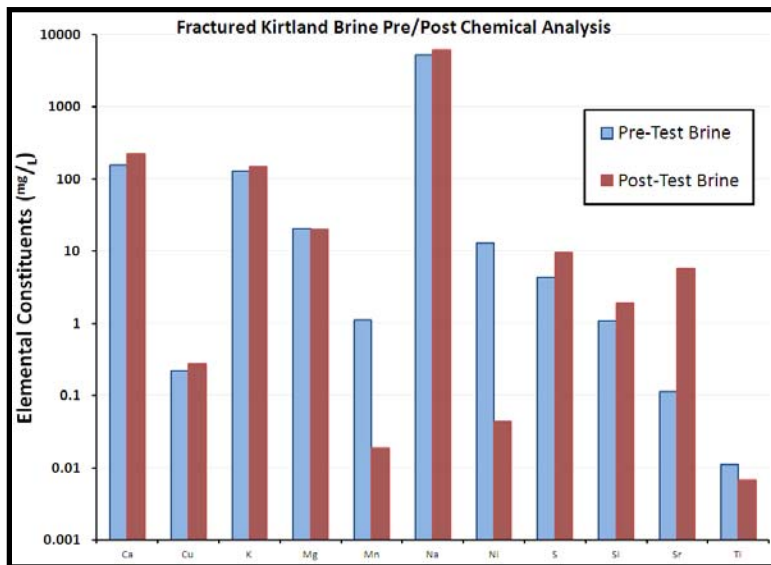


Figure 22: Pre- and post-elemental constituents in the brine used for the Kirtland shale fractured flow test.

The first test has shown a minimal amount of change in the fracture. The very low flow rate over this test (≈ 1 ml/day) was identified as a possible reason for this low amount of reaction. All future tests used an increased flow rate of at least 0.013 ml/min, or 18.72 ml/day.

4.2 EAU CLAIRE MUDSTONE

Both medical and industrial CT scans were performed prior to subcoring the as-received Eau Claire mudstone. A slice through the center of the reconstructed medical CT scan of the Eau Claire mudstone sample is shown in Figure 23. There are brighter zones at the edges of this image from reconstruction errors (beam hardening) that should be neglected, but the complex internal structure of this core is still apparent, with different density bedding planes perpendicular to the core orientation. The reconstructed industrial CT scan of this same core is shown in Figure 24, and similar variation of the bedding planes is observed. Again the higher resolution industrial CT scan with a voxel resolution of $78.4\ \mu\text{m}$ enabled more of the structure to be viewed within this 3.5-in. (8.89 cm) diameter bulk sample. The industrial scan shows more detail about the variations within the sample; fine grained uniform mudstone zones are shown as the darker gray layers while mudstone of varied density and grain size is shown as the lighter-toned, mottled gray layers. These variations did not cause an issue in the subcoring of this sample for flow testing, and the sub-samples were mechanically fractured perpendicular to the bedding planes as previously described.

XRF measurements were conducted on the entire Eau Claire core and are shown in Figure 25. Chemical elements within the core do not vary significantly over the length of the core. The core is visibly heterogeneous, and fairly consistent across the XY planes within the bedding layers, but overall structure of the core is fairly uniform at the elemental level.

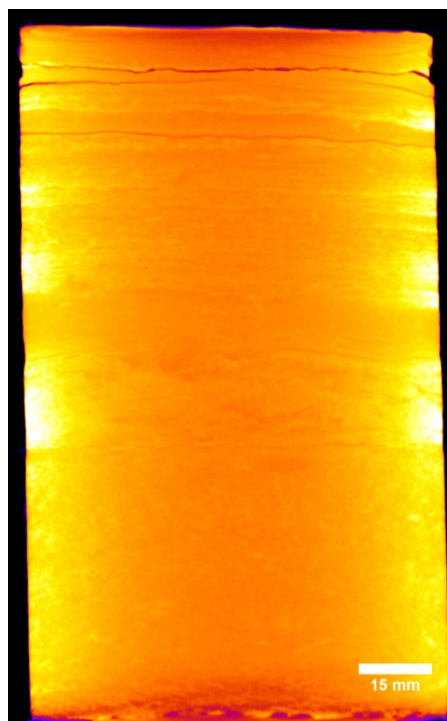


Figure 23: False color medical CT slice of full Eau Claire mudstone core, XZ plane.

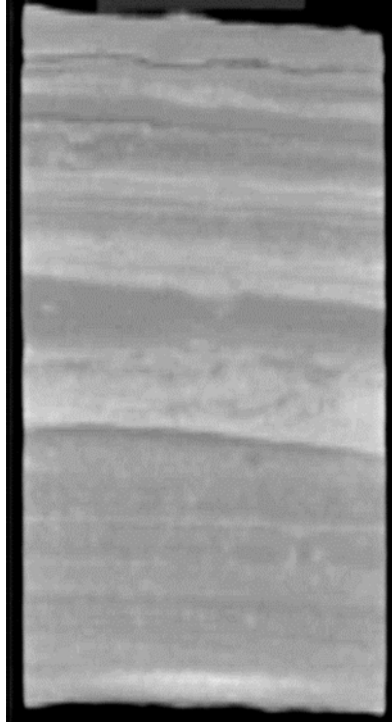


Figure 24: Greyscale industrial CT slice of full Eau Claire mudstone core, XZ plane.

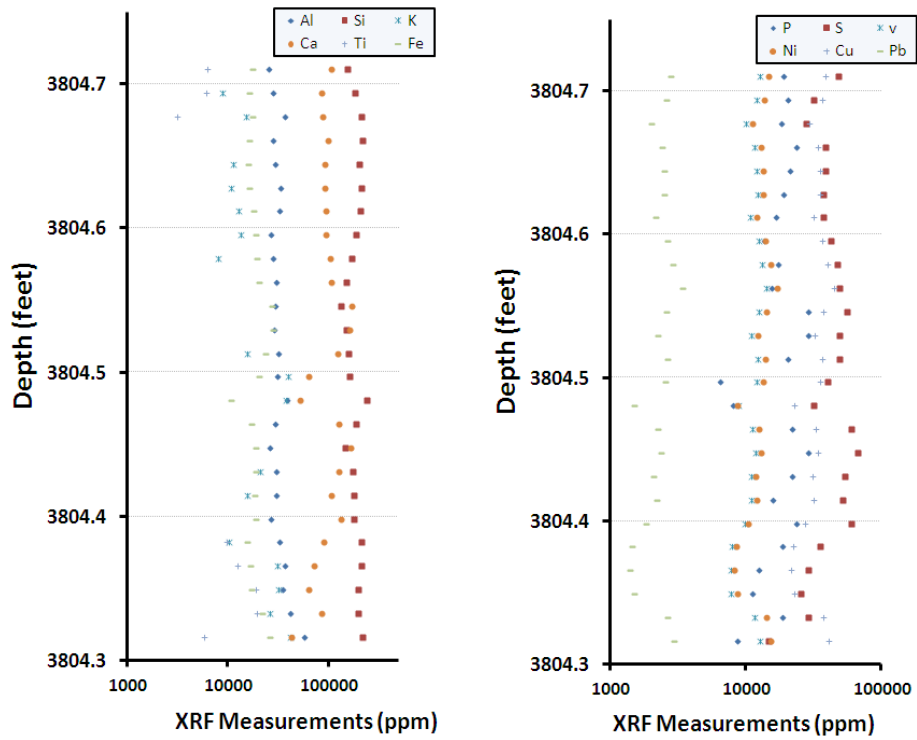


Figure 25: XRF measurements of the full Eau Claire mudstone core.

4.2.1 Eau Claire Sub-Core #1

An entire montage of medical CT scanner XY slices for the Eau Claire sub-core #1 is shown in Figure 26. The fracture is more apparent within this scan due to the mechanical fracturing of the sub-core along the length of the sample. Distinct variation in the density of the rock matrix due to the different bedding planes can be noted in Figure 26 by the changes from lighter to darker regions. This matches the variation in the full core seen in the previous CT scans and in visual observations. The purple slice in the upper left corner of Figure 26 is the end of the core where brine-saturated- CO_2 was injected. A higher resolution industrial CT scan was performed on this sub-core as well. The difference in CTN from the rock matrix to the open fracture volume was large enough to perform an isolation of the fracture from the reconstruction of the 3-D core volume (Figure 27). Several features of this fracture can be noted from Figure 26 and Figure 27. The fracture contains zero aperture zones, which are regions where the fracture walls touch. This type of contact between surfaces has been shown to dramatically affect the transmissivity of a fracture (Pyrak-Nolte and Morris, 2000). Also, there is a secondary fracture perpendicular to the primary fracture roughly $3/4$ of the distance from the injection side of the core. Neither of these features hindered flow through the fracture in a meaningful way and a constant injection rate of 0.013 ml/min was maintained for the entire experiment, with the pore pressure remaining around 1,650 psi.

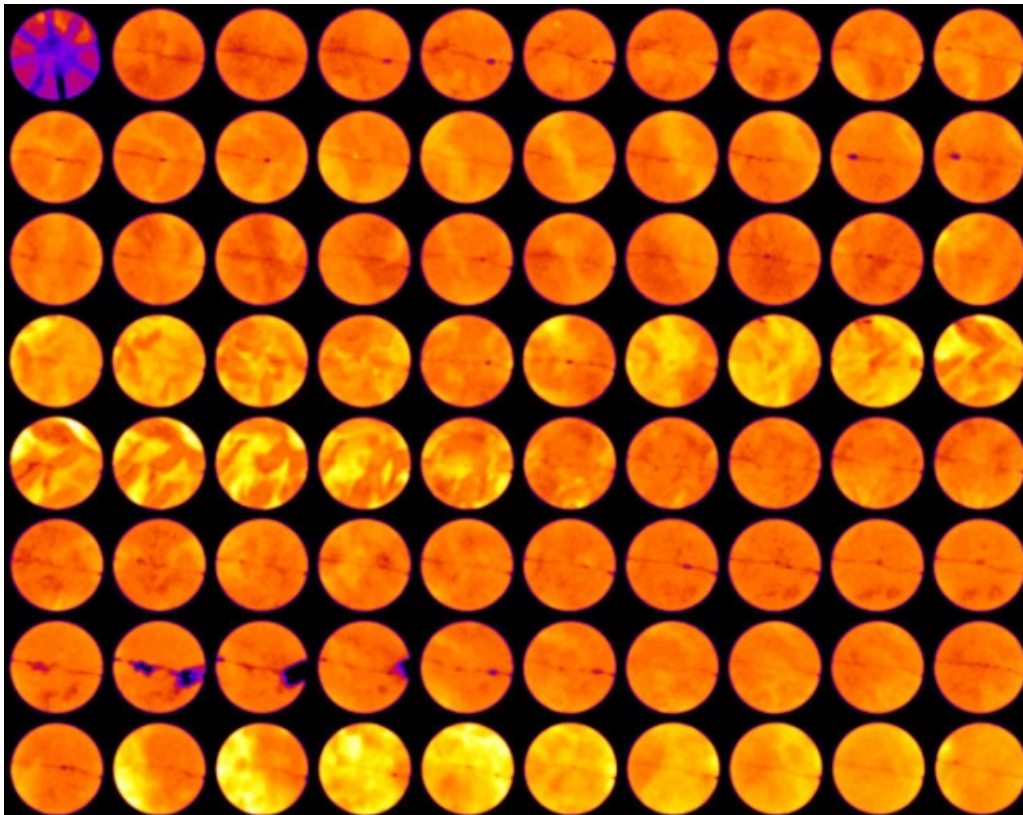


Figure 26: Slices of the medical CT scanner reconstruction of Eau Claire mudstone sub-core #1, XY plane.

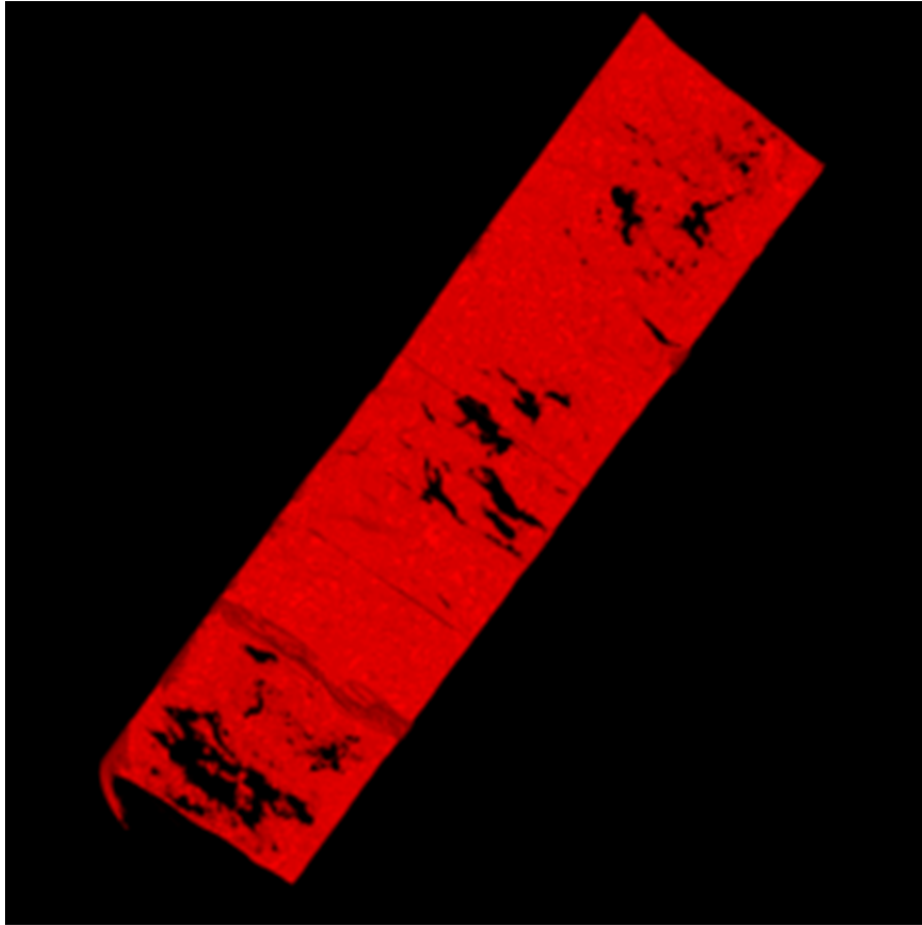


Figure 27: 3-D reconstruction of an industrial CT scan of the fracture in the Eau Claire mudstone sub-core #1.

Initial analysis of the CT scans show little change in the fracture structure over the 22-day-long experiment. The bulk density of the sample as derived from the CTN of the full XY slices from the medical CT scans showed no significant difference in the average density of the core over the duration of the test (Figure 28). The values plotted in Figure 28 have error bars showing +/- one standard deviation of the bulk density. There was a nominal increase in the density during the last week of the experiment, but the density decreased again by the end of the experiment. The scans during this period were examined to determine if there was some observable phenomenon that occurred in this time period. Though no direct causation was found, it is suspected that this change in the bulk density was due to environmental factors within the CT scanner building during this time.

A smaller region of interest that encompassed the primary fracture and less of the surrounding rock matrix was used to calculate the bulk density of a more focused zone around the fracture. This region of interest is shown in Figure 29. To confirm that the bulk material far from the fracture was not masking changes in the density around the fracture zone, the density was calculated and averaged for each scan on this smaller region. The results, in Figure 30, show that the density of this smaller region follows the same trends as the full core bulk density and that no conclusive information about changes to the fracture can be derived solely from the CT data.

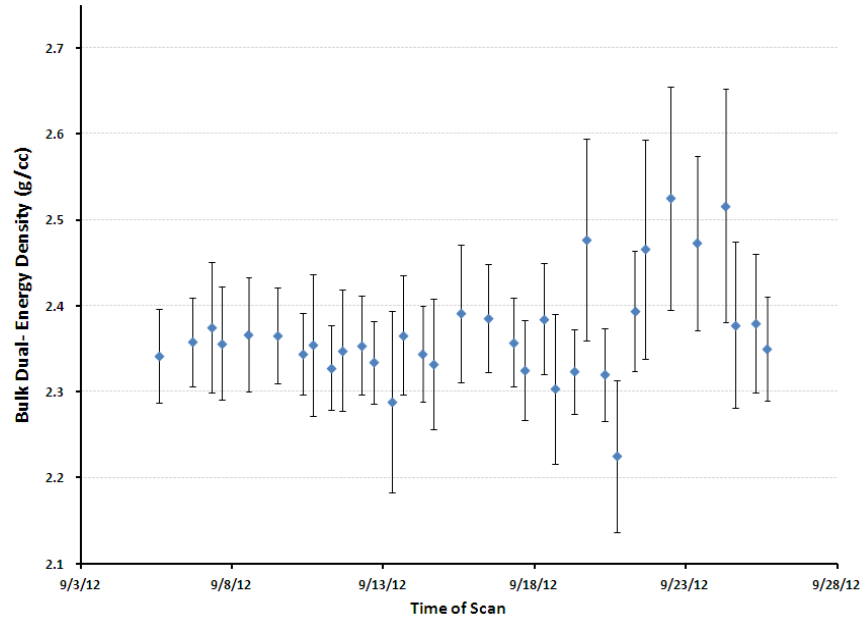


Figure 28: Averaged bulk dual-energy derived density of the entire of the Eau Claire sub-core #1.

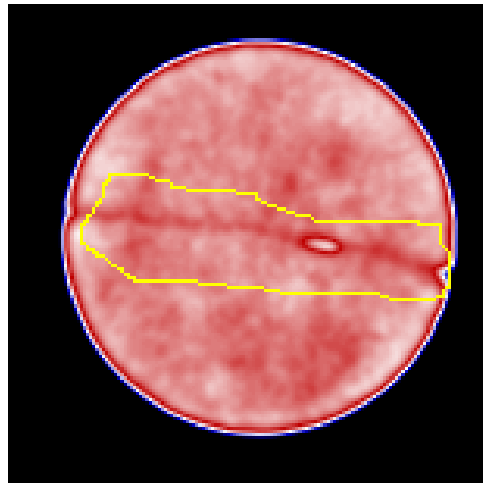


Figure 29: Fracture region of interest (shown in yellow) for analysis of Eau Claire sub-core #1.

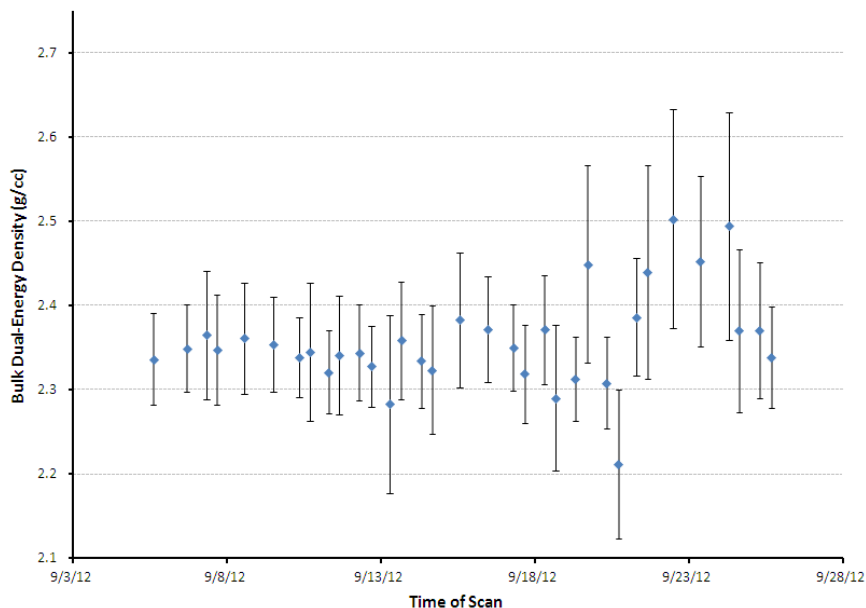


Figure 30: Averaged bulk dual-energy derived density of the smaller region of interest of the Eau Claire sub-core #1.

The pressure across this core was measured by a 0–250 psi differential pressure transducer during this test. Unfortunately, the LabView virtual instrument that recorded the data was calibrated to collect data from a different type of device. As such, no reliable pressure data was recorded during this test. No large change in the pressures was noted during the daily operation of the experiment.

4.2.2 Eau Claire Sub-Core #2

With multiple sub-cores of the same section of the Eau Claire (Figure 6), and the disappointing pressure measurements in the first Eau Claire fractured flow test, an additional test was performed with a similar fractured sample (Figure 7). Initially this flow rate was set to 0.013 ml/min. This fractured core was so permeable the low injection rate had a difficult time in maintaining the pore pressure of 1,650 psi, so after two days of operation the flow rate was increased to 0.026 ml/min.

The XY slice montage of the medical CT scan for the Eau Claire fractured core #2 is shown in Figure 31. In this representation, the primary fracture along the length of the core is shown vertically and in the center of the core. The XZ slice montage is shown in Figure 32 and has a similar bedding plane structure to Eau Claire fractured core #1, which is not surprising considering the bedding planes traverse the entire “as-received” core (Figure 24).

The medical CT scan derived dual-energy bulk density is shown in Figure 33. Very little variation in the density was observed over the course of this experiment. The outlying data point from the scan on October 20, 2012 was scanned on a weekend day, though the reason for the higher than average density from this scan is unclear. A linear fit to the data shows a very slight increase in the density with a slope of $4(10^{-4})$; removing the data from October 20 does not alter the slope of this fit. Similar to the Eau Claire test #1, no conclusive changes in the fracture structure can be determined from the medical CT images alone.

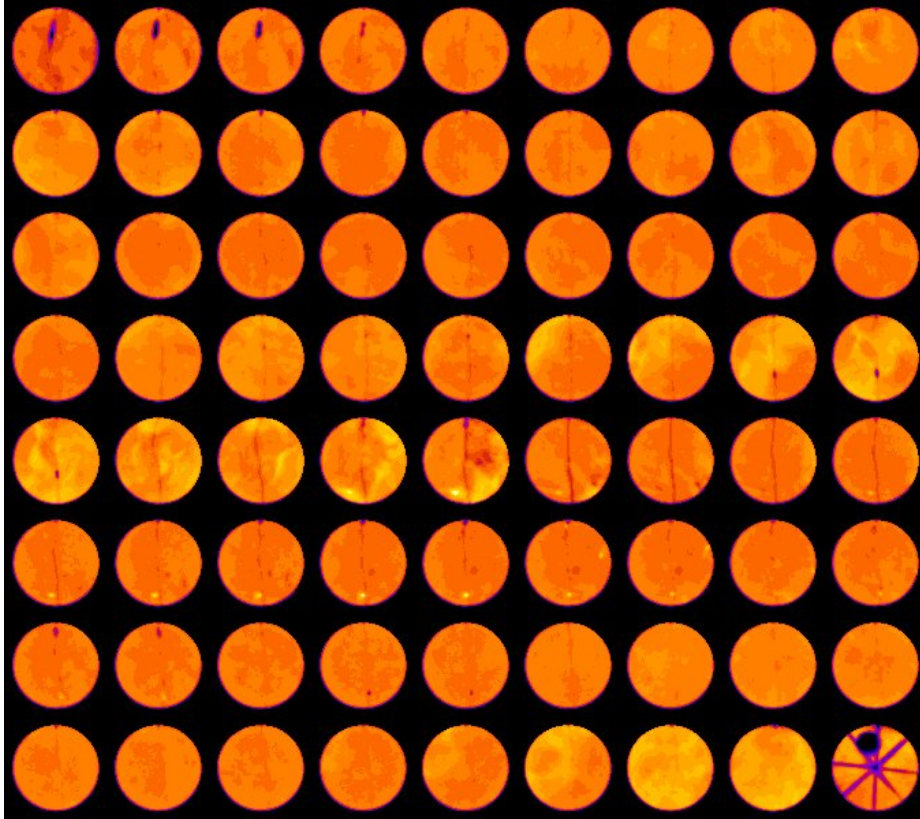


Figure 31: Slices of the medical CT scanner reconstruction of Eau Claire mudstone sub-core #2, XY plane.

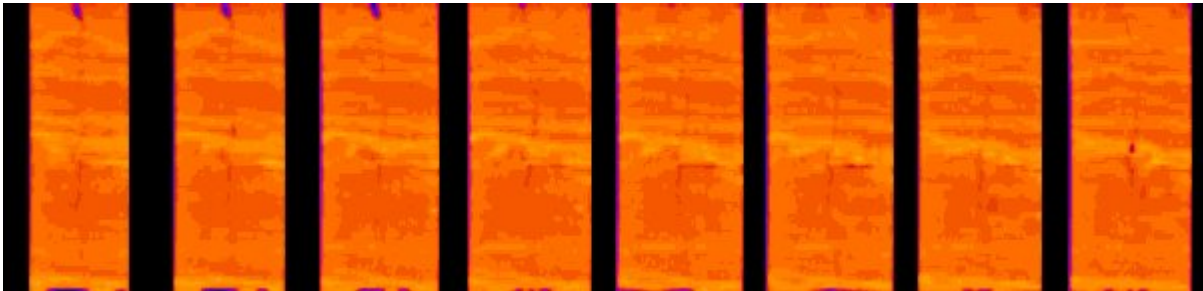


Figure 32: Slices of the medical CT scanner reconstruction of Eau Claire mudstone sub-core #2, XZ plane.

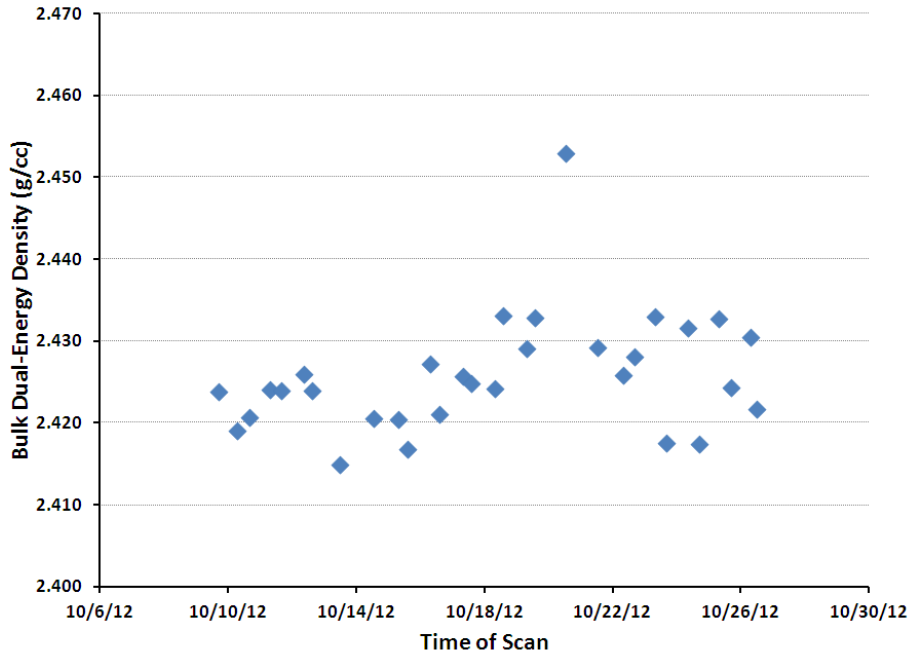


Figure 33: Averaged bulk dual-energy derived density of the entire Eau Claire sub-core #2.

The pressure across the core was measured with a Setra 0-250 differential pressure transducer and recorded with a LabView virtual instrument every 30 s. This recorded data was averaged over 20 min intervals and is shown in Figure 34 over the course of the experiment. There is a spread in the data between 1.3 and 2.1 (with one outlier at 1.07 psi), but the general trend is unchanging; a linear fit to the data has a slope of -10^{-4} . This lack of change in the pressure indicates that no measureable change in the differential pressure was recorded. The increase in the flow rate from 0.013 to 0.026 on day two of the experiment had no measurable effect on the recorded pressure either. This may be due to the low differential pressure being on the edge of the range of discernible pressures that the transducer could record.

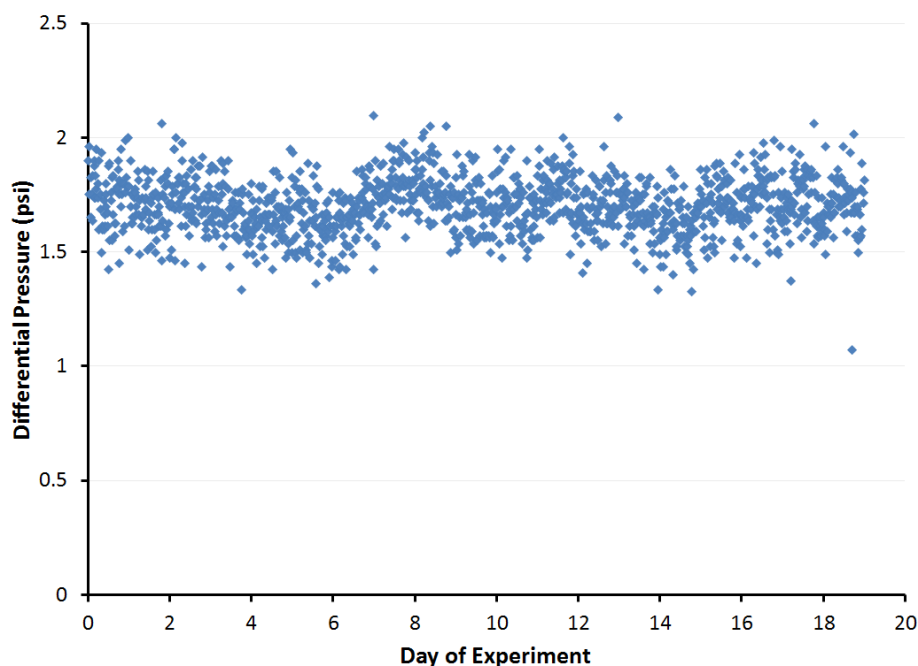


Figure 34: Pressure across Eau Claire sub-core #2, measured from 0–250 psi differential pressure gauge.

4.2.3 Tuscaloosa Claystone

The final test performed in this series of experiments used a Tuscaloosa claystone sample that was cut as a sidewall core. One bedding-parallel fracture could be seen in this core, and this fracture's origin, either natural or coring-induced, was not determined. This was the only core studied where flow was parallel to the bedding planes. No photographs of the core were obtained, though the structure of the core is similar to other sidewall cores from the same well (see, e.g., Figure 9).

The medical CT scanner XY slice montage of the fractured Tuscaloosa claystone is shown in Figure 35. The core is heterogeneous, with several higher density zones (light regions) and several fractures along the length of the core. The XZ slices shown in Figure 36 reveal a fracture at the base of the core that connects the end to the diameter of the core. The core was coated with epoxy prior to being placed in the rubber-sleeve and core holder, so “short-circuiting” of the fluid along the outside diameter was unlikely.

The dual-energy derived density again shows little in the way of observable trends. Several measurements were well below the average density of 2.72 g/cc. The CT scanner's machine errors may have contributed to these values. With the three outliers removed a linear fit has a slope of 10^{-4} , and thus no changes to the geometry of the core were detectable from the medical CT images alone.

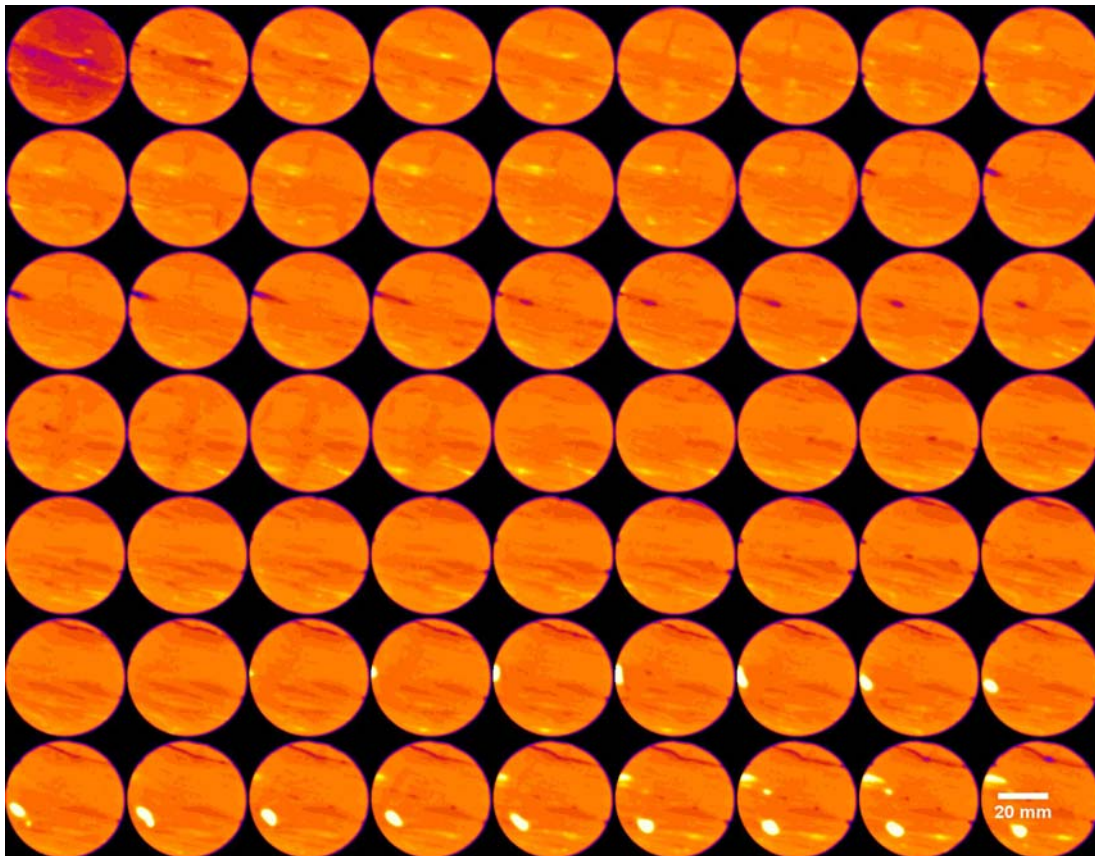


Figure 35: False color medical CT slices of fractured Tuscaloosa claystone sample, XY planes.

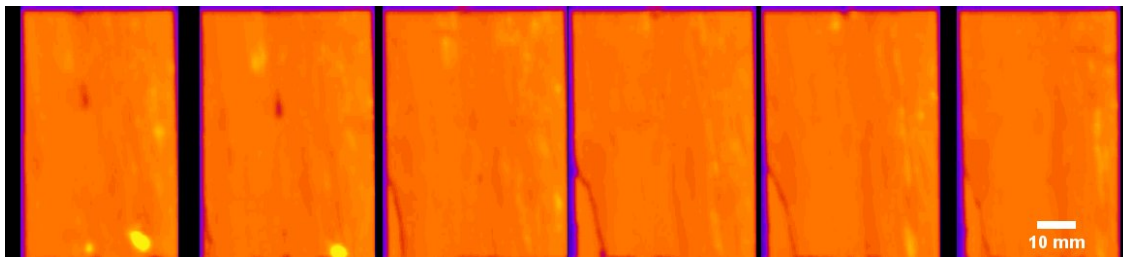


Figure 36: False color medical CT slices of fractured Tuscaloosa claystone sample, XZ planes.

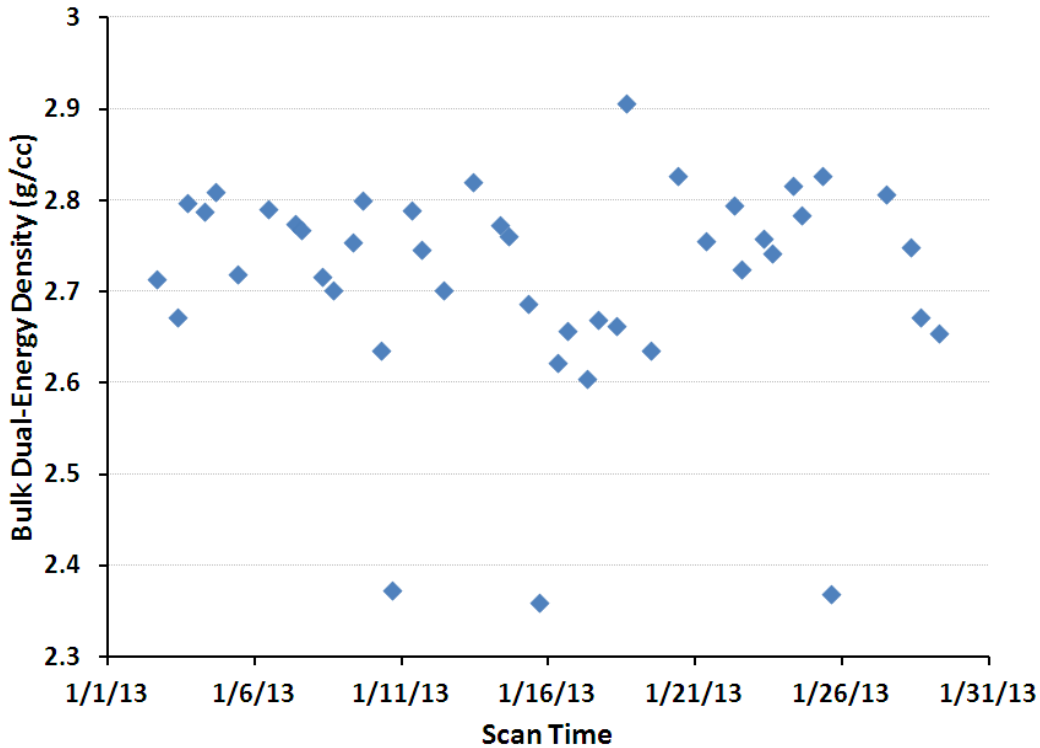


Figure 37: Averaged bulk dual-energy derived density of the Tuscaloosa claystone.

The pressure differential across the core was recorded every 30 s with the same pressure transducer and LabView recording system used for the Eau Claire #2 sample. The values averaged every 20 min are shown in Figure 38. A noticeable increase in the pressure differential from ≈ 3.3 psi to ≈ 4.4 psi was observed. This could be an indication of small amounts of precipitation within the fracture voids that reduced the mechanical and hydraulic aperture of the fracture, an excellent trait for a sealing formation. Alternatively, it could indicate the two sides of the fracture were slowly being forced closer to each other by the confining stress applied external to the sample, perhaps with the aid of dissolution of asperities that had propped the fracture open.

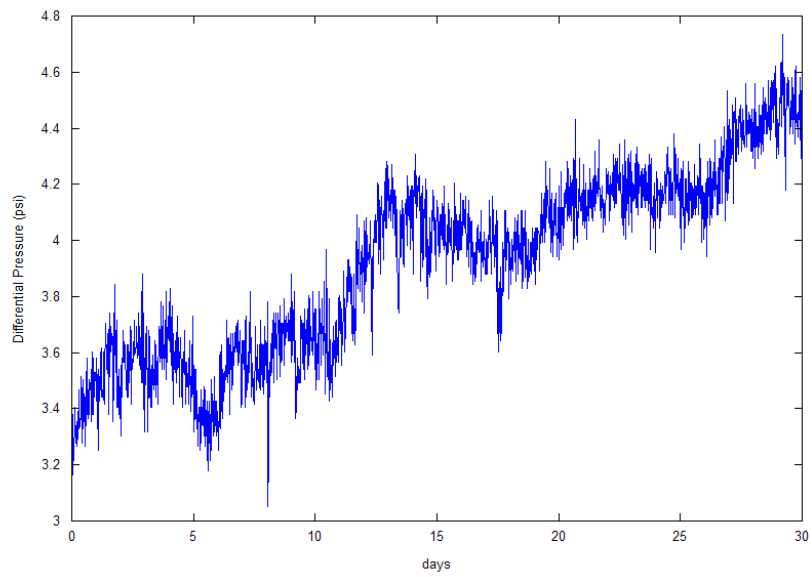


Figure 38: Pressure across the Tuscaloosa fractured core, measured from 0–250 psi differential pressure gauge.

5. DISCUSSION

For the three formations studied, there was a minimal change in the recorded fracture properties over the course of the saturated CO₂-brine flow experiments. This was a good result, indicating that the potential sealing properties of these formations will not degrade when in contact with CO₂-saturated brine. Even though these were long tests for laboratory studies, on the geologic scale of interest for CCUS activities they are short. As such, longer experiments may yield different results.

In addition, three of the four experiments were at room temperature due to issues with the temperature control mechanism in the test apparatus. An increase in the temperature of the cores and fluids may increase the reaction rate and promote more rapid alteration of the fracture structure.

The most dramatic change was the reduction in the hydraulic aperture of the Tuscaloosa fractured sample, as shown by the increase in the differential pressure across the core. This observed increase in the resistance to flow deserves further investigation. No other flow properties were observed to change as much. Some comments on how the individual experiments could be improved are mentioned below.

5.1 KIRTLAND SHALE

A follow-up experiment may be warranted with very similar conditions. The brine used was a mixture of NaCl, MgCl, and KCl based upon USGS measurements of in situ brines at the depth from which this sample was obtained in the San Juan Basin. But, CaCl, which did show up in the USGS reports, was not added to the experimental brine. An increase in the injection rate of the fluids and proper pressure recording could also provide more definite results from this experiment.

5.2 EAU CLAIRE MUDSTONE

Previous experimental studies of the Eau Claire under CO₂ sequestration conditions indicate that little reactivity would be expected (Liu et al., 2012). Our study observed this as well. Longer tests at elevated temperature conditions may provide additional insights, but the Eau Claire appears to have excellent rock properties to serve as a non-reactive, sealing formation for geologic CO₂ sequestration or storage.

5.3 TUSCALOOSA CLAYSTONE

The Tuscaloosa sample was the only one to react in a measurable fashion, with the apparent slight reduction in fracture transmissivity. A test through a core that was fractured perpendicular to the bedding planes (as would be the case in fracture that would provide a leakage path from a CCUS facility) might be a worthwhile experiment. In addition, elevated temperature, similar to what would be expected in situ, could increase the rate of reactions.

6. CONCLUSIONS

Four samples from three different geologic formations were studied with the finding that only one sample had a reaction that may be significant. Apparently, either reactions or compression within the fracture of the Tuscaloosa claystone sample reduced the transmissivity of the fracture slightly over the 39-day experiment. The apparent change in the geometry of the fracture was not sufficient to be observed with the medical CT images. All other tests showed a minimal amount of change in the fracture and fracture flow properties.

The lack of change in the hydraulic properties of the fractures indicate that the non-dynamic pressure to flow relationships discussed in the introduction and currently implemented in many discrete fracture flow models is adequate to describe the flow of CO₂-saturated brine through fractured seals. That is, there appears to be little need for the inclusion of geochemical alterations to the basic fracture flow equations when the reactivity of the surrounding rock matrix material is very low. When other factors affect the behavior of a fracture (such as changes to the stress field) those factors may need to be included, but there appears to be minimal geochemical reactions between the seal formations studied and the CO₂-brine mixtures used in these experiments.

Several methods for improving the experiments are listed in the discussion section of this report. In particular, using a higher resolution scanner *may* provide additional insight into geometric changes and performing the tests at a higher temperature *may* increase the rate of reactions between the fluids and the rock.

7. REFERENCES

- Arora, S.; Acharya, J.; Verma, A.; Panigrahi, P. K. Multilevel thresholding for image segmentation through a fast statistical recursive algorithm. *Pattern Recognition Letter* **2008**, *29*, 119–125. DOI:10.1016/j.patrec.2007.009.005
- Barrett, J. F.; Keat, N. Artifacts in CT: Recognition and Avoidance. *RadioGraphics* **2004**, *24*, 1679–1691. <http://dx.doi.org/10.1148/rg.246045065>
- Bear, J. *Dynamics of Fluids in Porous Media*; American Elsevier Publishing, 1972.
- Berkowitz, B. Characterizing flow and transport in fractured geological media: A review. *Adv Water Res* **2002**, *25*, 861–884.
- Brown, B.; Nereth, K. J.; Rhudy, R.; Esposito, R. Southeast Regional Carbon Partnership (SECARB) *The Mississippi Test Site* Fact Sheet. www.secarbon.org (accessed May 2013).
- Carroll, S. A.; McNab, W. W.; Dai, Z.; Torres, S. C. Reactivity of Mount Simon Sandstone and the Eau Claire Shale under CO₂ storage conditions. *Environ. Sci. Technol.* **2012**, *47*, 252–261. <http://dx.doi.org/10.1021/es301269k>
- Crandall, D.; Bromhal, G.; Karpyn, Z. T. Numerical simulations examining the relationship between wall-roughness and fluid flow in fractures. *Int. J. Rock Mech. Mining Sci.* **2010**, *47*, 784–796. <http://dx.doi.org/10.1016/j.ijrmms.2010.03.015>
- Deng, H.; Ellis, B. R.; Peters, C. A.; Fitts, J.; Crandall, D.; Bromhal, G. Modification of carbonate fracture hydrodynamic properties by CO₂-acidified brine flow. *Energy Fuels* **2013a**, *27*, 4221–4231. <http://dx.doi.org/10.1021/ef302041s>
- Deng, H.; Fitts, J.; Peters, C. A.; Li, L.; Crandall, D.; Bromhal, G. Experimental study of permeability evolution of an Eau Claire fracture exposed to CO₂ rich brine. 47th U.S. Rock Mechanics/Geomechanics Symposium, San Francisco, CA, June 23–26, 2013; 2013b.
- Detwiler, R. L.; Rajaram, H. Predicting dissolution patterns in variable aperture fractures: Evaluation of an enhanced depth-averaged computational model. *Water Resour. Res.* **2007**, *43*, W04403. <http://dx.doi.org/10.1029/2006WR005147>
- Durham, W. B.; Bourcier, W. L.; Burton, E. A. Direct observation of reactive flow in a single fracture. *Water Resour. Res.* **2001**, *37*, 1–12. <http://dx.doi.org/10.1029/2000WR900228>
- Ellis, B. R.; Bromhal, G. S.; McIntyre, D. M.; Peters, C. A. Changes in caprock integrity due to vertical migration of CO₂-enriched brine. *Energy Proceed* **2011**, *4*, 5327–5334. <http://dx.doi.org/10.1016/j.egypro.2011.02.514>
- Fazio, J. URS. Personal communication, 2012.
- Gouze, P.; Noiriél, C.; Bruderer, C.; Loggia, D.; Leprovost, R. X-ray tomography characterization of fracture surfaces during dissolution. *Geophy. Res. Lett.* **2003**, *30*, 1267. <http://dx.doi.org/10.1029/2002GL016755>
- Griffith, C. A.; Dzombak, D. A.; Lowry, G. V. Physical and chemical characteristics of potential seal strata in regions considered for demonstrating geological saline CO₂ sequestration. *Environ. Earth Sci.* **2011**, *64*, 925–948. <http://dx.doi.org/10.1007/s12665-011-0911-5>

- Haerer, D.; McPherson, B. Evaluating the impacts and capabilities of long term subsurface storage in the context of carbon sequestration in the San Juan basin, NM and CO. *Energy Procedia* **2009**, *1*, 2991–2998. <http://dx.doi.org/10.1016/j.egypro.2009.02.076>
- Heath, J. E.; McPherson, B. J. O. L.; Dewers, T. A. *Natural Tracers and Multi-Scale Assessment of Caprock Sealing Behavior: A Case Study of the Kirtland Formation, San Juan Basin*; Technical Report for the U.S. Department of Energy; DOE Award No.: DE-FC26-05NT42591; U.S. Department of Energy, 2010; p 184. <http://dx.doi.org/10.2172/1025536>
- Huerta, N. J.; Hesse, M. A.; Bryant, S. L.; Strazisar, B. R.; Lopano, C. L. Experimental evidence for self-limiting reactive flow through a fractured cement core: Implications for the time-dependent wellbore leakage. *Environ. Sci. Technol.* **2013**, *47*, 269–275. <http://dx.doi.org/10.1021/es3013003>
- ICCP. *Contribution of Working Group III to the Fourth Assessment Report of the Intergovernmental Panel on Climate Change*; Metz, B., Davidson, O. R.; Bosch, P. R., Dave, R., Meyer, L. A., Eds.; Cambridge University Press: Cambridge, United Kingdom and New York, NY, 2007.
- Jain, J. URS. Personal communication, 2012.
- Jikich, S. A.; McIntyre, D.; Bromhal, G. S.; Crandall, D. Mechanical properties, flow properties, and heterogeneous CO₂ sorption in confined Powder River Basin coal cores. 44th US Rock Mechanics Symposium and 5th US-Canada Rock Mechanics Symposium, Salt Lake City, UT, June 27–30, 2010.
- Keller, J. Terra Tek. Personal communication, 2009.
- Konzuk, J. S.; Kueper, B. H. Evaluation of cubic law based models describing single-phase flow through a rough-walled fracture. *Water Resour. Res.* **2004**, *40*, W02402. <http://dx.doi.org/10.1029/2003WR002356>
- Li, L.; Steefel, C. I.; Yang, L. Scale dependence of mineral dissolution kinetics within single pores and fractures. *Geochimica Et Cosmochimica Acta* **2008**, *72*, 360–377. doi:10.1016/j.gca.2007.10.027
- Liu, F.; Lu, P.; Griffith, C.; Hedges, S. W.; Soong, Y.; Hellevang, H.; Zhu, C. CO₂-brine-caprock interaction: Reactivity experiments on Eau Claire shale and a review of relevant literature. *Int. J. of Greenhouse Gas Contr.* **2012**, *7*, 153–167. <http://dx.doi.org/10.1016/j.ijggc.2012.01.012>
- Lu, J.; Milliken, K.; Reed, R. M.; Hovorka, S. Diagenesis and sealing capacity of the middle Tuscaloosa mudstone at the Cranfield carbon dioxide injection site, Mississippi, U.S.A. *Environ. Geosci.* **2011**, *18*, 35–53. <http://dx.doi.org/10.1306/eg.09091010015>
- Lu, J.; Kharaka, Y. K.; Thordsen, J. J.; Horita, J.; Karamalidis, A.; Griffith, C.; Hakala, J. A.; Ambats, G.; Cole, D. R.; Phelps, T. J.; Manning, M. A.; Cook, P. J.; Hovorka, S. D. CO₂-rock brine interactions in Lower Tuscaloosa Formation at Cranfield CO₂ sequestration site, Mississippi, U.S.A. *Chem. Geol.* **2012**, *291*, 269–277. <http://dx.doi.org/10.1016/j.chemgeo.2011.10.020>

- McCord, J.; Reiter, M.; Phillips, F. Heat-flow data suggest large ground-water fluxes through Fruitland coals of the northern San Juan basin, Colorado-New Mexico. *Geology* **1992**, *20*, 419–422.
- NETL. *The United States 2012 Carbon Utilization and Storage Atlas*, 4th ed.; Department of Energy, National Energy Technology Laboratory; pp 130.
<http://www.netl.doe.gov/File%20Library/Research/Coal/carbon-storage/atlasiv/Atlas-IV-2012.pdf>
- Noiriel, C.; Luquot, L.; Madé, B.; Raimbault, L.; Gouze, P.; van der Lee, J. Changes in reactive surface area during limestone dissolution: An experimental and modelling study. *Chem. Geol.* **2009**, *265*, 160–170. <http://dx.doi.org/10.1016/j.chemgeo.2009.01.032>
- Osuna-Enciso, V.; Cuevas, E.; Sossa, H.; A comparison of nature inspired algorithms for multi-threshold image segmentation. *Expert Systems with Applications* **2013**, *40*, 1213–1219. DOI:10.1016/j.eswa.2012.08.017
- Pawar, R.; Bromhal, G.; Dilmore, R.; Foxall, B.; Jones, E.; Oldenburg, C.; Stauffer, P.; Unwin, S.; Guthrie, G. *Quantification of Risk Profiles for Atmospheres and Groundwater*; NRAP-TRS-III-003-2013; NRAP Technical Report Series; U.S. Department of Energy, National Energy Technology Laboratory: Morgantown, WV, 2013; p 28.
- Peters, C. A. Accessibilities of reactive minerals in consolidated sedimentary rock: An imaging study of three sandstones. *Chem. Geol.* **2009**, *265*, 198–208.
<http://dx.doi.org/10.1016/j.chemgeo.2008.11.014>
- Pyrak-Nolte, L. J.; Cook, N. G. W.; Nolte, D. D. Fluid percolation through single fractures. *Geophys Res. Lett.* **1988**, *15*, 1247–1250. <http://dx.doi.org/10.1029/GL015i011p01247>
- Pyrak-Nolte, L. J.; Morris, J. P. Single fractures under normal stress: The relation between fracture specific stiffness and fluid flow. *Int. J. Rock Mech. Min. Sci.* **2000**, *37*, 245–262.
[http://dx.doi.org/10.1016/S1365-1609\(99\)00104-5](http://dx.doi.org/10.1016/S1365-1609(99)00104-5)
- Reeves, S. R. The Coal-Seq project: Key results from field, laboratory and modeling studies. Proceedings of the 7th International Conference on Greenhouse Gas Control Technologies (GHGT-7), Vancouver, Canada, September 5, 2004; pp 1399-1406.
- Santarosa, C. S.; Crandall, D.; Haljasmaa, I. V.; Hur, T.-B.; Fazio, J. J.; Warzinski, R. P.; Heemann, R.; Ketzer, J. M. M.; Romanov, V. N. CO₂ sequestration potential of Charqueadas coal field in Brazil. *Int. J. Coal Geol.* **2013**, *106*, 25–34.
<http://dx.doi.org/10.1016/j.coal.2013.01.005>
- Sullivan C.; Gilmore, T.; Horner, J.; Kelley, M.; Appriou, D.; Hoffman, J. Update on the FutureGen2.0 characterization well activities in Morgan County, Illinois. Presented at the 11th Annual Conference on Carbon Capture, Utilization, & Sequestration, Pittsburgh, PA April 30–May 3, 2012.
- Walsh, J. B. The effect of pore pressure and confining pressure on fracture permeability. *Int. J. Rock Mech.* **1981**, *18*, 429–435. [http://dx.doi.org/10.1016/0148-9062\(81\)90006-1](http://dx.doi.org/10.1016/0148-9062(81)90006-1)
- Wellington, S. L.; Vinegar, H. J. Tomographic imaging of three-phase flow experiments. *Rev. Sci. Instr.* **1987**, *58*, 96–107.

- Wilson, T. H.; Wells, A.; Peters, D.; Mioduchowski, A.; Martinez, G.; Koperna, G.; Akwari, B. N.; Heath, J. Fracture and 3D seismic interpretations of the Fruitland Formation and cover strata: Implications for CO₂ retention and tracer movement, San Juan Basin Pilot test. *Int. J. Coal Geol.* **2012**, *99*, 35–53. <http://dx.doi.org/10.1016/j.coal.2012.02.007>
- Witherspoon, P. A.; Amick, C. H.; Gale, J. E.; Iwai, K. Observations of a potential size effect in experimental determination of the hydraulic properties of fractures. *Water Resour. Res.* **1979**, *15*, 1142–1146. <http://dx.doi.org/10.1029/WR015i005p01142>
- Witherspoon, P. A.; Wang, J. S. Y.; Iwai, K.; Gale, J. E. Validity of Cubic Law for fluid flow in deformable rock fracture. *Water Resour. Res.* **1980**, *16*, 1016–1024. <http://dx.doi.org/10.1029/WR016i006p01016>
- Zhang, Y.; Pau, G. [*Reduced-order model development for CO₂ storage in brine reservoirs*](#); NRAP-TRS-III-005-2012; NRAP Technical Report Series; U.S. Department of Energy, National Energy Technology Laboratory: Morgantown, WV, 2012; p 20.
- Zimmerman, R. W.; Chen, D.-W.; Cook, N. G. W. The effect of contact area on the permeability of fractures. *J. Hydrol.* **1992**, *139*, 79–96. [http://dx.doi.org/10.1016/0022-1694\(92\)90196-3](http://dx.doi.org/10.1016/0022-1694(92)90196-3)
- Zimmerman, R. W.; Bodvarsson, G. S. Hydraulic conductivity of rock fractures. *Trans. Porous Media* **1996**, *23*, 1–30. <http://dx.doi.org/10.1007/BF00145263>



NRAP is an initiative within DOE's Office of Fossil Energy and is led by the National Energy Technology Laboratory (NETL). It is a multi-national-lab effort that leverages broad technical capabilities across the DOE complex to develop an integrated science base that can be applied to risk assessment for long-term storage of carbon dioxide (CO₂). NRAP involves five DOE national laboratories: NETL Regional University Alliance (NETL-RUA), Lawrence Berkeley National Laboratory (LBNL), Lawrence Livermore National Laboratory (LLNL), Los Alamos National Laboratory (LANL), and Pacific Northwest National Laboratory (PNNL). The NETL-RUA is an applied research collaboration that combines NETL's energy research expertise in the Office of Research and Development (ORD) with the broad capabilities of five nationally recognized, regional universities—Carnegie Mellon University (CMU), The Pennsylvania State University (PSU), University of Pittsburgh (Pitt), Virginia Polytechnic Institute and State University (VT), and West Virginia University (WVU)—and the engineering and construction expertise of an industry partner (URS Corporation).

Technical Leadership Team

Jens Birkholzer

LBNL Technical Coordinator
Lawrence Berkeley National Laboratory
Berkeley, CA

Grant Bromhal

NETL Technical Coordinator
Lead, Reservoir Performance Working Group
Office of Research and Development
National Energy Technology Laboratory
Morgantown, WV

Chris Brown

PNNL Technical Coordinator
Pacific Northwest National Laboratory
Richmond, WA

Susan Carroll

LLNL Technical Coordinator
Lawrence Livermore National Laboratory
Livermore, CA

Josh White

Lead, Induced Seismicity Working Group
Lawrence Livermore National Laboratory
Livermore, CA

Diana Bacon

Lead, Groundwater Protection Working Group
Pacific Northwest National Laboratory
Richmond, WA

Tom Daley

Lead, Strategic Monitoring Working Group
Lawrence Berkeley National Laboratory
Berkeley, CA

George Guthrie

Technical Director, NRAP
Office of Research and Development
National Energy Technology Laboratory
Pittsburgh, PA

Rajesh Pawar

LANL Technical Coordinator
Lead, Systems/Risk Modeling Working Group
Los Alamos National Laboratory
Los Alamos, NM

Tom Richard

Deputy Technical Director, NRAP
The Pennsylvania State University
NETL-Regional University Alliance
State College, PA

Nik Huerta

Lead, Migration Pathways Working Group
Office of Research and Development
National Energy Technology Laboratory
Albany, OR



Sean Plasynski
Director
Strategic Center for Coal
National Energy Technology Laboratory
U.S. Department of Energy

John Wimer
Director
Office of Coal and Power R&D
National Energy Technology Laboratory
U.S. Department of Energy

Susan Maley
Technology Manager
Crosscutting Research
National Energy Technology Laboratory
U.S. Department of Energy

Mark Ackiewicz
Director
Division of Carbon Capture and Storage
Office of Fossil Energy
U.S. Department of Energy

NRAP Executive Committee

Cynthia Powell
Director
Office of Research and Development
National Energy Technology Laboratory
U.S. Department of Energy

Alain Bonneville
Laboratory Fellow
Pacific Northwest National Laboratory

Donald DePaolo
Chair, NRAP Executive Committee
Associate Laboratory Director
Energy and Environmental Sciences
Lawrence Berkeley National Laboratory

Melissa Fox
Program Manager
Applied Energy Programs
Los Alamos National Laboratory

Roger Aines
Chief Energy Technologist
Lawrence Livermore National
Laboratory

George Guthrie
Technical Director, NRAP
Office of Research and Development
National Energy Technology Laboratory

